The photodetachment-modulated electron capture detector
by Robert Stephen Mock

A thesis submitted in partial fulfillment of the requirements for the degree of Doctor of Philosophy in Chemistry
Montana State University

Abstract:
Photodetachment (PD) of electrons from negative ions in a pulsed electron capture detector (ECD) is described. Sensitive responses to halogenated hydrocarbons that produce I-, Br-, or Cl- upon electron capture can be produced by passing a chopped light beam through the ECD and amplifying the modulated component of the signal. The photodetachment-modulated (PDM) ECD can be made to respond selectively and sensitively to iodine-containing hydrocarbons alone or to iodine- and bromine-containing hydrocarbons in the presence of chlorinated hydrocarbons. This capability is shown to be useful in the trace analysis of a complex mixture of halogenated hydrocarbons by gas chromatography. The PD spectra of Cl-, Br-, and I-and the absolute PD cross-section for I" at 365 nm are reported and are in excellent agreement with previous measurements by other methods.

Low resolution, electron PD spectra of the molecular radical anions of nitrobenzene and 30 other nitroaromatic hydrocarbons bearing methyl, fluoro, chloro, bromo, and cyano substituents are reported for the first time. Absolute PD cross-sections over the spectral range 300 to 1200 nm have been obtained. These molecules undergo PD by two mechanisms, Direct PD and Resonance PD. Through measurements of Direct PD, the minimum photon energy necessary to cause PD has been determined for each anion and compared with adiabatic electron affinities determined previously by gas phase electron transfer equilibria. Resonance PD spectra for many anions is compared to UV-Vis absorption spectra previously measured in gamma-irradiated frozen glasses. Through Resonance PD, peak maxima of high absolute cross-section are observed. Where the PD cross-section is small compared to the absorption cross-section at peak maxima, low quantum efficiency for Resonance PD is thought to result from poor Franck-Condon overlap.

By measuring the decrease in the PD response to azulene with increasing temperature, an electron autodetachment rate has been determined and is found to be consistent with previous results obtained in a pulsed high pressure mass spectrometer. The PDM-ECD has also been shown to be useful in determining the branching ratios of EC for CBrCl3 and CCl4. Results also show that the neutral radicals, CC13 and CBrCl2 . can undergo EC at low temperatures, but at higher temperatures are destroyed by well reactions

THE PHOTODETACHMENT-MODULATED ELECTRON CAPTURE DETECTOR

by

Robert Stephen Mock

A thesis submitted in partial fulfillment
of the requirements for the degree

of

Doctor of Philosophy

in

Chemistry

MONTANA STATE UNIVERSITY
Bozeman, Montana

March 1989

APPROVAL

of a thesis submitted by

Robert Stephen Mock

This thesis has been read by each member of the thesis committee and has been found to be satisfactory regarding content, English usage, format, citations, bibliographic style, and consistency, and is ready for submission to the College of Graduate Studies.

2/24/89
Date

Eric Dumsnil
Chairperson, Graduate Committee

Approved for the Major Department

2/24/89
Date

Edwin H Abbott
Head, Major Department

Approved for the College of Graduate Studies

3/9/89
Date

Henry L Parsons
Graduate Dean

STATEMENT OF PERMISSION TO USE

In presenting this thesis in partial fulfillment of the requirements for a doctoral degree at Montana State University, I agree that the Library shall make it available to borrowers under rules of the Library. I further agree that copying of this thesis is allowable only for scholarly purposes, consistent with "fair use" as prescribed in the U.S. Copyright Law. Requests for extensive copying or reproduction of this thesis should be referred to University Microfilms International, 300 North Zeeb Road, Ann Arbor, Michigan 48106, to whom I have granted "the exclusive right to reproduce and distribute copies of the dissertation in and from microfilm and the right to reproduce and distribute by abstract in any format."

Signature Robert Stephen Mork

Date 2/24/89

ACKNOWLEDGEMENT

I would like to thank the current and past members of the research group, especially Berk Knighton, Doug Zook, and Joe Sears, who were all tremendously helpful, and who are also good friends. I thank my advisor, Dr. Eric Grimsrud, for making my work here meaningful and productive. I thank my parents for instilling in me a life-long pursuit of learning, and for providing moral support. I thank my brother, Alan, for providing encouragement by "leading the way" through graduate school. Lastly, my gratitude to and love for Jan, Joshua, and Suzanne cannot be expressed in words. I thank them the most.

TABLE OF CONTENTS

TABLE OF CONTENTS-Continued

LIST OF TABLES

LIST OF FIGURES

LIST OF FIGURES-Continued

LIST OF FIGURES-Continued

LIST OF FIGURES-Continued

ABSTRACT

Photodetachment (PD) of electrons from negative ions in a pulsed electron capture detector (ECD) is described. Sensitive responses to halogenated hydrocarbons that produce I^-, Br^-, or Cl^- upon electron capture can be produced by passing a chopped light beam through the ECD and amplifying the modulated component of the signal. The photodetachment-modulated (PDM) ECD can be made to respond selectively and sensitively to iodine-containing hydrocarbons alone or to iodine- and bromine-containing hydrocarbons in the presence of chlorinated hydrocarbons. This capability is shown to be useful in the trace analysis of a complex mixture of halogenated hydrocarbons by gas chromatography. The PD spectra of Cl^-, Br^-, and I^- and the absolute PD cross-section for I^- at 365 nm are reported and are in excellent agreement with previous measurements by other methods.

Low resolution, electron PD spectra of the molecular radical anions of nitrobenzene and 30 other nitroaromatic hydrocarbons bearing methyl, fluoro, chloro, bromo, and cyano substituents are reported for the first time. Absolute PD cross-sections over the spectral range 300 to 1200 nm have been obtained. These molecules undergo PD by two mechanisms, Direct PD and Resonance PD. Through measurements of Direct PD, the minimum photon energy necessary to cause PD has been determined for each anion and compared with adiabatic electron affinities determined previously by gas phase electron transfer equilibria. Resonance PD spectra for many anions is compared to UV-Vis absorption spectra previously measured in gamma-irradiated frozen glasses. Through Resonance PD, peak maxima of high absolute cross-section are observed. Where the PD cross-section is small compared to the absorption cross-section at peak maxima, low quantum efficiency for Resonance PD is thought to result from poor Franck-Condon overlap.

By measuring the decrease in the PD response to azulene with increasing temperature, an electron autodetachment rate has been determined and is found to be consistent with previous results obtained in a pulsed high pressure mass spectrometer. The PDM-ECD has also been shown to be useful in determining the branching ratios of EC for $CBrCl_3$ and CCl_4. Results also show that the neutral radicals, CCl_3 and $CBrCl_2$, can undergo EC at low temperatures, but at higher temperatures are destroyed by wall reactions.

INTRODUCTION

Since its introduction in the 1950's, the electron capture detector (ECD) has been the most common gas chromatographic (GC) detector for the determination of environmental samples. This is due to the fact that the gas-phase electron attachment rates for many molecules of environmental interest are very fast while the attachment rates for many hydrocarbons, a large but uninteresting portion of most environmental samples, are relatively slow. The ECD can then provide a sensitive and selective detection technique requiring a minimum of sample clean-up or preparation. For example, detection and measurement of atmospheric halocarbons in relatively clean air has been accomplished by GC-ECD by injections of whole air samples (1-3). More complicated samples containing tens or hundreds of hydrocarbons with significant electron capture coefficients can create more of a detection problem. The inherent selectivity of the ECD may not be enough to provide accurate identification of the compounds present. In such cases, a more selective or intelligent detection system must be used, such as mass spectrometry.

Recently, the versatility of the ECD for a wide variety of analyses has been greatly improved by what may collectively be called the chemically sensitized (CS) ECD. By the intentional addition of oxygen (4, 5) or nitrous oxide (6) to the carrier gas, the ECD can respond to classes of compounds which do not capture electrons rapidly under normal conditions. The intentional addition of ethyl chloride to the carrier gas has been shown to enhance the ECD response to compounds of low electron affinities, such as anthracene (7). Although the CS-ECD improves the sensitivity to some classes of compounds, it is not yet known whether chemical sensitization will assist in the analysis of complex samples. What is needed for complex samples is an induced perturbation of the ECD signal, which, when detected and amplified, provides an additional element of specificity towards sample components of interest. One means of creating a perturbation of this type is the introduction of light-induced photodetachment (PD), Reaction 1, into the ECD. Ideally, this electron

$$M^- + h\nu \longrightarrow M + e \qquad (1)$$

capture-photodetachment detector would respond only to those compounds which 1) rapidly capture thermalized electrons, and 2) form negative ions which will readily undergo photodetachment at a selected wavelength.

Electron photodetachment from atomic and polyatomic anions has proven to be a useful means of studying thermochemical and spectroscopic properties of negative ions and their photoproducts (8-12). The photodetachment spectra of numerous atomic (13-18) and polyatomic (19-26) negative ions have previously been reported. The PD process is a transition from a bound electron in the anion to a free continuum electron and the neutral. The minimum energy required to induce PD is equal to the electron affinity (EA) of the neutral. Hence, PD has been extensively used for the measurement of gas phase electron affinities (27). Since electron affinities seldom exceed 4 eV, visible and near-UV light sources can be used to induce PD. The PD spectra of polyatomic negative ions has also been shown to provide information concerning the excited states of the negative ions and the neutral products.

Photodetachment spectra are often broad and relatively featureless. For atomic negative ions, such as the halides shown in Figure 1, the increase in cross-section, σ, with photon energy is very abrupt in the region of the EA-determined threshold. The most significant difference between the PD spectra of I^-, Br^-, and Cl^- shown in Figure 1 is the differing onsets of PD corresponding to the EA of each halide ion.

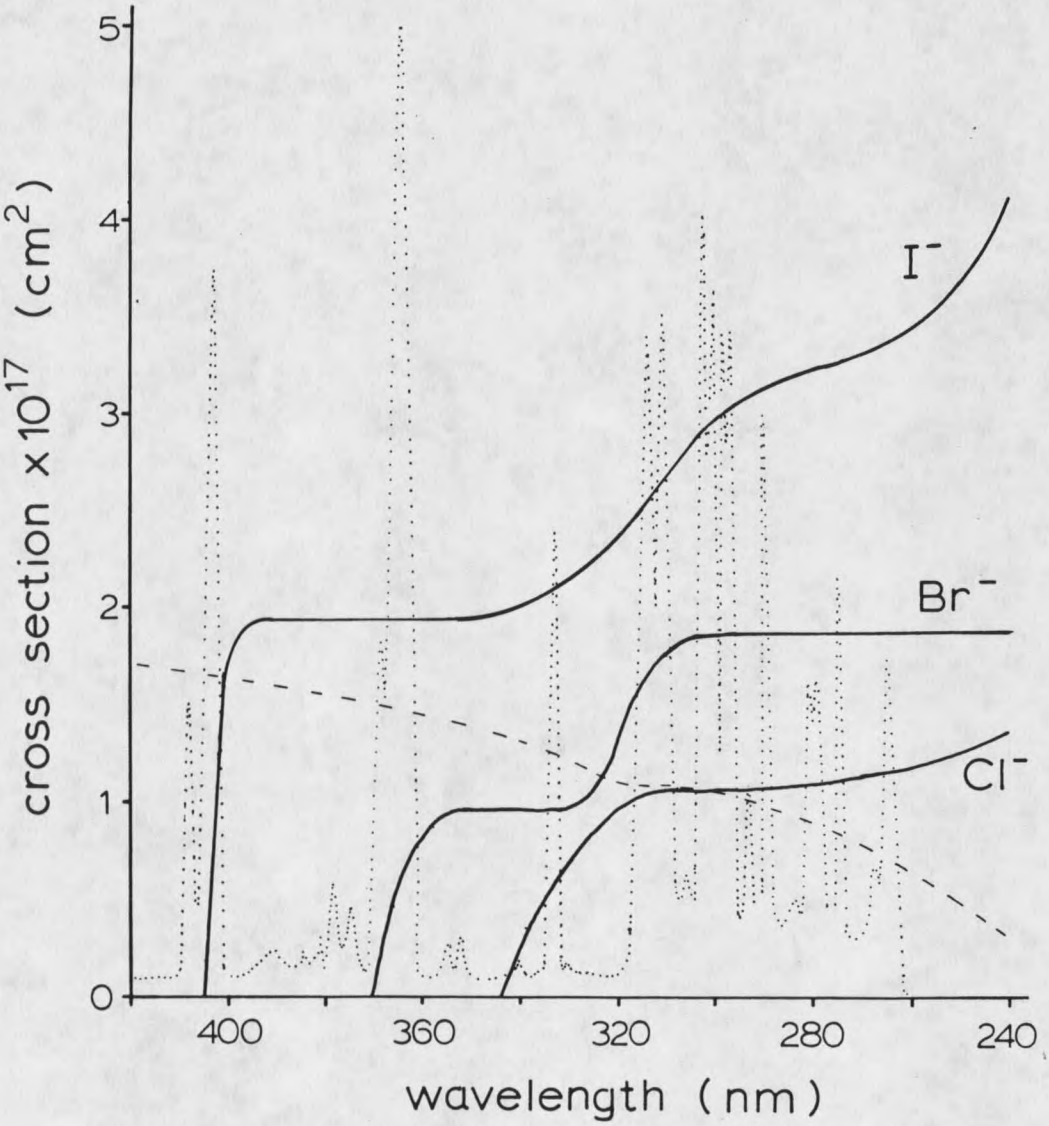

Figure 1. Photodetachment spectra and cross-sections of iodide, bromide, and chloride negative ions (reproduced from references 13 and 14). Also shown are the emission spectra of a Xe (dashed line) and a Hg/Xe (dotted line) arc lamp.

The PD spectra of polyatomic anions tend to exhibit a gradual increase in σ with increasing photon energy in the threshold region. This gradual increase is expected due to the added complexities associated with the numerous vibronic and rotational states that are accessible to the polyatomic anion and the neutral product. Also, differences in the geometries of the negative ion and the neutral (Franck-Condon overlap) can greatly complicate the PD spectra of polyatomic anions.

In the previously mentioned studies of PD, measurements were generally made by one of two approaches. For most studies involving atomic anions, measurements were made utilizing shock tubes. For example, Mandl (13, 14) introduced cesium halides into nitrogen gas and subjected the gas sample to shock heating, causing the cesium halide to ablate and dissociate, forming positive ions and negative halide ions. This method produces very high ion densities, on the order of 10^{16} ions/cm^3. Ultraviolet light produced by a Xe flash lamp is introduced into the shock tube containing the ions and the absorption of light measured. The absorption is due to PD of the negative halide ions; so the magnitude of the absorption is proportional to the PD cross-section of the anion.

For polyatomic anions, the most common approach has been that involving the ion cyclotron resonance mass

spectrometer (ICR-MS) in conjunction with a light source (8, 11). This technique involves the measurement of the diminution by light of mass spectrometrically generated ion beams. Although the ICR-MS is well-suited to the study of PD due to its ability to generate a variety of mass-identified negative ions and then to trap and study them for relatively long periods of time, there are certain inherent limitations. First, the internal energy of the negative ions produced in an ICR cavity is generally not under tight experimental control, which can complicate the interpretation of PD spectra (8, 11). The negative ions are typically formed by energetic chemical means and the excess internal energy imparted to the product ions is not efficiently removed by collisions in the 10^{-8} to 10^{-5} Torr environment of the ICR cavity (28-30). This is especially severe when an anion is formed by resonance electron capture, Reaction 2, from a molecule, M, of high electron affinity. Since the EA of

$$e + M \longrightarrow M^{-*} \qquad (2)$$

molecules which readily lead to negative ions can be quite high, occasionally exceeding 3eV, the internal energy imparted to the molecular anion, M^{-*} by Reaction 2 will be correspondingly high.

A second problem can arise in ICR-MS photodetachment studies if the natural lifetime of the initially-formed

excited anion, M^{-*}, is too short against autodetachment, the reverse of Reaction 2. For example, Christophorou (31) has shown that the lifetimes of the molecular negative ions of nitrobenzene and substituted nitrobenzenes formed by capture of low-energy electrons are on the order of tens of microseconds. Since stabilizing collisions can occur in an ICR cavity no faster than about one per millisecond, the natural lifetimes of these initially-formed negative ions may not be sufficiently long as to allow their PD spectra to be reliably measured. Perhaps for this reason, the PD spectra of only a few molecular radical anions have been reported by the ICR method. If the lifetime is sufficiently long, a PD spectrum may be obtained. An example is the study of the resonance electron capture product of SF_6. For this anion, a PD experiment was reported by the ICR-MS (32) and appears to have been made possible by the existence of one of several excited states of SF_6^{-*} which has an unusually long lifetime against autodetachment (31, 33-35). Most of the PD measurements of polyatomic negative ions reported by the ICR-MS method have been performed on negative ions formed by dissociative electron capture reactions or by ion-molecule reactions in which an even electron anion is irreversibly formed.

In 1983, Dovichi and Keller (36) described the use of an ECD for the measurement of the PD spectrum of NO_2^- at atmospheric pressure. In that experiment, a line-tunable argon-ion laser producing up to 3W of continuous power in the selected wavelengths was used in conjunction with a direct current (DC) ECD. With this instrument, PD-modulated (PDM) ECD responses to NO_2^- were observed. Although the PDM signals were weak, they were sufficiently strong as to provide a PD spectrum of NO_2^- that was consistent with the known PD spectrum. In that study, the low PDM-ECD sensitivity can be partially attributed to the small PD cross-section for NO_2^- at the wavelengths used; at 488 nm, $\sigma = 4x10^{-19}$ cm^2 (26). Also, low sensitivity may have resulted from the use of a DC-ECD. The basic operational principles of a DC-ECD are not well understood (37). In particular, the location and lifetimes of negative ions within a DC-ECD are unknown.

With a pulsed ECD, it is possible to describe more clearly the dynamics occurring within the ionization volume. Several details of this description point to potential advantages of the pulsed ECD over the DC-ECD for its application to PD. For example, it is known that the lifetimes of the negative ions formed within a pulsed ECD are relatively long and these ions will be concentrated in a predictable location within the

ionization volume by a positive ion-space charge field (38, 39). If a cylindrical ionization cell is used, the negative ions formed will be contained along its central axis (39). If a light beam is then passed through this same region of the cell, the interaction of negative ions and photons will be maximized. Since most of the important ECD processes which effect the measured electron current can be modeled with a reasonable level of accuracy, a relatively detailed understanding of the quantitative response of the PDM-pulsed ECD should be possible. Using these models, it may be possible to determine absolute, as well as relative, PD cross-sections for negative ions formed in the ECD.

There are also inherent advantages to using the PDM-pulsed ECD specifically for the PD studies of molecular anions. In particular, the molecular anions of nitroaromatic hydrocarbons are readily formed in an ECD by electron capture, Reaction 2. These excited state molecular anions are then rapidly quenched by collisions with the atmospheric pressure buffer gas, B, as shown in Reaction 3. This process overwhelms autodetachment, the

$$M^{-*} \xrightarrow{B} M^{-} \qquad (3)$$

reverse of reaction 2. Also, at atmospheric pressure, Reaction 3 is sufficiently effective in removing excess internal energy from the negative ions that the ions are

almost certainly in thermal equilibrium with the buffer gas. This should greatly simplify the interpretation of PD spectra and allow meaningful comparisons between PDM-pulsed ECD results and those of previous studies of the thermodynamic and spectroscopic properties of the corresponding ground state anions.

THEORY

With a thorough understanding of the processes occurring within the ECD, it should be possible to predict and understand the qualitative and quantitative responses to various molecules. The model to be discussed here is the same as models for the pulsed ECD described elsewhere (38, 40) with the addition of the photodetachment reaction. The important reactions occurring within the ECD which should adequately explain and determine the magnitude of the electron population between pulses are shown as Reactions 4-8.

$$N_2 \xrightarrow{ß} p^+ + e \qquad (4)$$

$$e + p^+ \xrightarrow{R_e} \text{neutrals} \qquad (5)$$

$$e + MX \xrightarrow{k_e} X^- + M \qquad (6a)$$

$$e + M \xrightarrow{k_e} M^- \qquad (6b)$$

$$X^- + P^+ \xrightarrow{R_{X-}} \text{neutrals} \qquad (7)$$

$$X^- + hv \xrightarrow{k_{hv}} X + e \qquad (8)$$

The ion chemistry occurring within the ECD is initiated by continuous beta radiation emitted by a ^{63}Ni-

on-Pt foil which forms the cylindrical walls of the cell (38). The secondary electrons created by this radiation are rapidly thermalized in the atmospheric pressure buffer gas and are contained within the central region of the reaction volume by a positive ion space-charge field (38, 39). The rate coefficient, ß, for this process is found by measuring the maximum standing current obtained at a very rapid pulse frequency in the absence of sample (41). In the ECD used in this study, ß = 1.87×10^{10} ion pairs s^{-1}. A measure of the average electron density existing within the cell is continuously provided by the fixed-frequency, pulsed method of ECD operation (38) in which all free electrons are periodically collected at the anode by a positive voltage pulse.

Reaction 5 is the recombination of electrons with positive ions. For a given detector, the product of the rate coefficient, R_e, and the positive ion density, n_+, can be determined from measurements of standing current as a function of pulse frequency (41). For this detector at 100°C, $R_e n_+ = 300$ sec^{-1}.

When a molecule of high electron affinity enters the cell, some of the electrons will be captured to form stable negative ions. Reaction 6a represents dissociative electron capture, which, in this study, leads to the formation of I^-, Br^-, or Cl^-. Resonance electron capture is represented by Reaction 6b. In this

case, which is actually the sum of Reactions 2 and 3, stable molecular ions are formed. (In the following discussion of the kinetic fate of the negative ions, X^- will be used as the negative ion representation. However, the molecular ion M^- has the same fate. Later, when the spectra of the ions are addressed, distinctions will be made as to exact identity.) Both Reactions 6a and 6b will decrease the average electron population within the cell. The first order rate of electron loss by either Reaction 6a or 6b will be given by the product, $k_e n_{mx}$. The negative ions formed will also be contained within the central region of the ECD by the positive ion space charge and will not be lost by non-chemical means such as wall neutralization or ventilation out of the cell.

In the absence of light, all negative ions will be lost by recombination with positive ions, represented by Reaction 7. The pseudo-first-order rate coefficient, $R_{x-} n_+$, will be of major importance in predicting the magnitude of PD perturbations of the ECD response since Reaction 7 and Reaction 8 will compete directly for the available negative ions, X^-. If destruction of X^- occurs by Reaction 7, only neutrals are formed, and the loss of an electron from the system caused by Reaction 6 will be measured by the electrometer. If, however, X^- is destroyed by Reaction 8, an electron is regenerated and

the electron capture event is not detected by the electrometer.

The rate coefficient, $R_{x-}n_+$, for Reaction 7 cannot be measured directly by an ECD. An estimate of its magnitude can be made, however, based on the measurement of $R_e n_+$ from Reaction 5. Prior studies of atmospheric pressure ionization in a ^{63}Ni source have shown an increase in total positive ion density whenever the source is altered from an electron-dominated to a negative ion-dominated system by the introduction of a high concentration of an electron capturing substance (5, 42). The magnitude of this increase in total positive ion signal has been between 50 and 100%. This effect appears to be independent of the electron capturing substance used. Since the density of positive ions within a field-free atmospheric pressure ion source is thought to be determined by recombination reactions, the above observations should reflect the relative magnitudes of R_e and R_{x-}. More precisely, the total positive ion densities should be inversely proportional to the square root of the recombination coefficients involved (38, 42). These observations then lead to the following estimate: R_{x-} is expected to be one-half to one-fourth as large as R_e. This is consistent with other data. At atmospheric pressure, ion-ion recombination coefficients tend to a constant value of about 1×10^{-6} cm^3 s^{-1} (43). Positive

ion-electron recombination coefficients can exceed this value if the positive ions are cluster ions. The electron recombination coefficients of the cluster ions, $H^+(H_2O)_2$ and $H^+(H_2O)_3$, are 2 x 10^{-6} and 4 x 10^{-6} cm^3 s^{-1}, respectively (44, 45). Cluster ions of the type $H^+(H_2O)_n$ are commonly observed in atmospheric pressure ion sources (46), and the two cluster ions indicated, where n=2 and n=3, are the ones expected in relatively dry carrier gas. The following assessment now seems reasonable: when a small amount of MX enters the ECD, the small population of X^- which is created will recombine with positive ions at a rate described by $R_{x^-}n_+ \approx 1/3\ R_e n_+$. Since $R_e n_+$ in this ECD is 300 s^{-1}, a reasonable approximation is that $R_{x^-}n_+ = 100 \pm 50\ s^{-1}$.

The rate coefficient for Reaction 8 is given by $k_{hv} = \sigma\Phi$, where σ is the PD cross section and Φ is the light flux. If a negative ion, such as I^- shown in Figure 1, has σ = 2 x 10^{-17} cm^2 and is irradiated with 1.0 W cm^{-2} of 380 nm light (Φ = 2.0 x 10^{-18} photons cm^{-2} s^{-1}), then k_{hv} = 40 s^{-1}. Comparing this k_{hv} value to $R_{x^-}n_+$ = 100 s^{-1}, it is clear that reaction 8 can compete effectively with Reaction 7. In this particular case, almost one-third of the negative ions, X^-, will be photodetached by the light. This large a perturbation of the ECD processes should be easily measurable.

The expected response perturbations when PD is introduced into the ECD are shown in Figure 2 and are plotted as a function of the magnitude of k_{hv}. Although the magnitudes of the k_{hv} values shown are relatively large, the lower portion of the range should be readily achievable for favorable systems. Four types of ECD responses are shown in Figure 2, all of which can be measured with the instrumentation to be described in the Experimental Section. δI_N is the normal ECD response expected with no light present. δI_L is the response expected when a beam of light is continuously passed through the ECD. $\delta I_M'$ is the PD-modulated component of the ECD response expected when a chopped light beam passes through the cell. In the calculation of $\delta I_M'$, it is assumed that the dynamic processes occurring within the ECD are on a very fast time scale compared to the chopping frequency. The actual PD-modulated response, δI_M , is not identical to the predicted $\delta I_M'$. This issue will be addressed later. From Figure 2, it is seen that $\delta I_M' = \delta I_N - \delta I_L$. $\delta I_{L/C}$ is the ECD response expected when a chopped light beam is passed through the cell. $\delta I_{L/C}$ is equal to the average of δI_N and δI_L, and closely approximates δI_N when k_{hv} is small. All of the predicted responses were calculated with a personal computer by numeric integration of the processes described in Reactions 4-8 using the previously stated rate

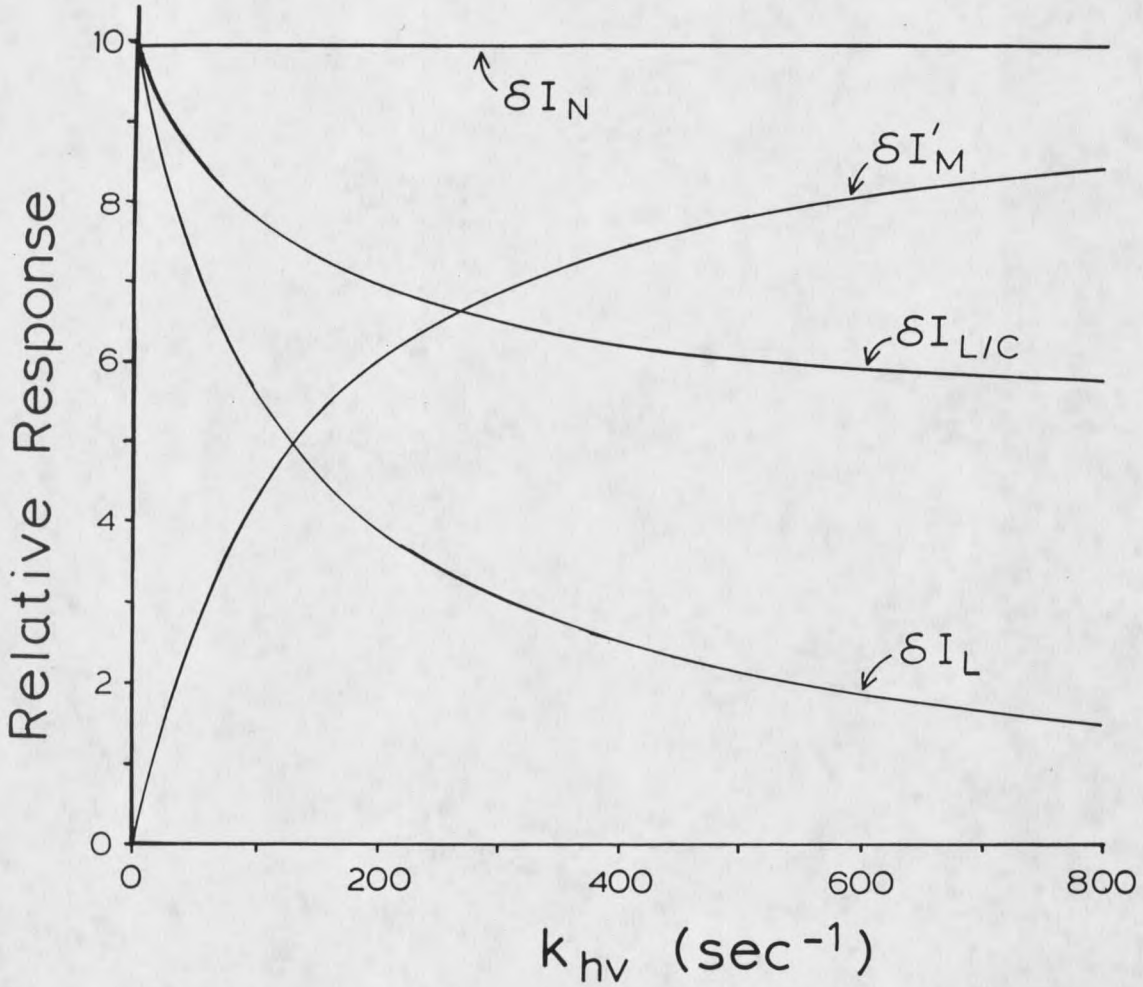

Figure 2. Theoretically predicted effects of photodetachment and its associated rate coefficient, k_{hv}, on the δI_N, δI_L, $\delta I_{L/C}$, and δI_M, responses of the pulsed ECD. Calculated from a model including Reactions 4-8 for which the following rate coefficients were used: ß = 1.87×10^{10} ion pairs s^{-1}, $R_e n_+ = 300\ s^{-1}$, $R_{x^-} n_+ = 100\ s^{-1}$. While $k_e n_{mx} = 100\ s^{-1}$ and a pulse frequency of 2 kHz are used, predictions of relative responses are independent of the magnitudes chosen for these parameters.

coefficients. A description of the program, along with a flow-chart and listing, are provided in Appendix A. Although values of $k_e n_{mx} = 100\ s^{-1}$ and a pulse frequency of 2KHz were used in these calculations, the results are independent of these parameters. Boundary conditions used in these calculations are that the population of electrons grows during each period between electron-removing pulses from zero to some positive value, and that the population of negative ions is the same at the beginning and end of each pulse period. In these calculations, the choice of sample size has no effect on the relative responses indicated in Figure 2 as long as sample size is kept small, so that no δI responses greater than 10% of the standing current occur. Within this low-sample range, all responses are predicted to be proportional to sample concentration.

Figure 2 predicts that over most of the range of k_{hv} values shown, PD should induce very significant and easily measurable perturbations of ECD responses. The magnitude of the modulated response, $\delta I_M'$, can easily be made 10% as great as the normal ECD response, δI_N. At higher k_{hv} values, the predicted response curve for $\delta I_M'$ becomes less steep and additional increases in light intensity have smaller effects.

In curve A of Figure 3, the ratio of the predicted $\delta I_M'$ and $\delta I_{L/C}$ responses are plotted as a function of

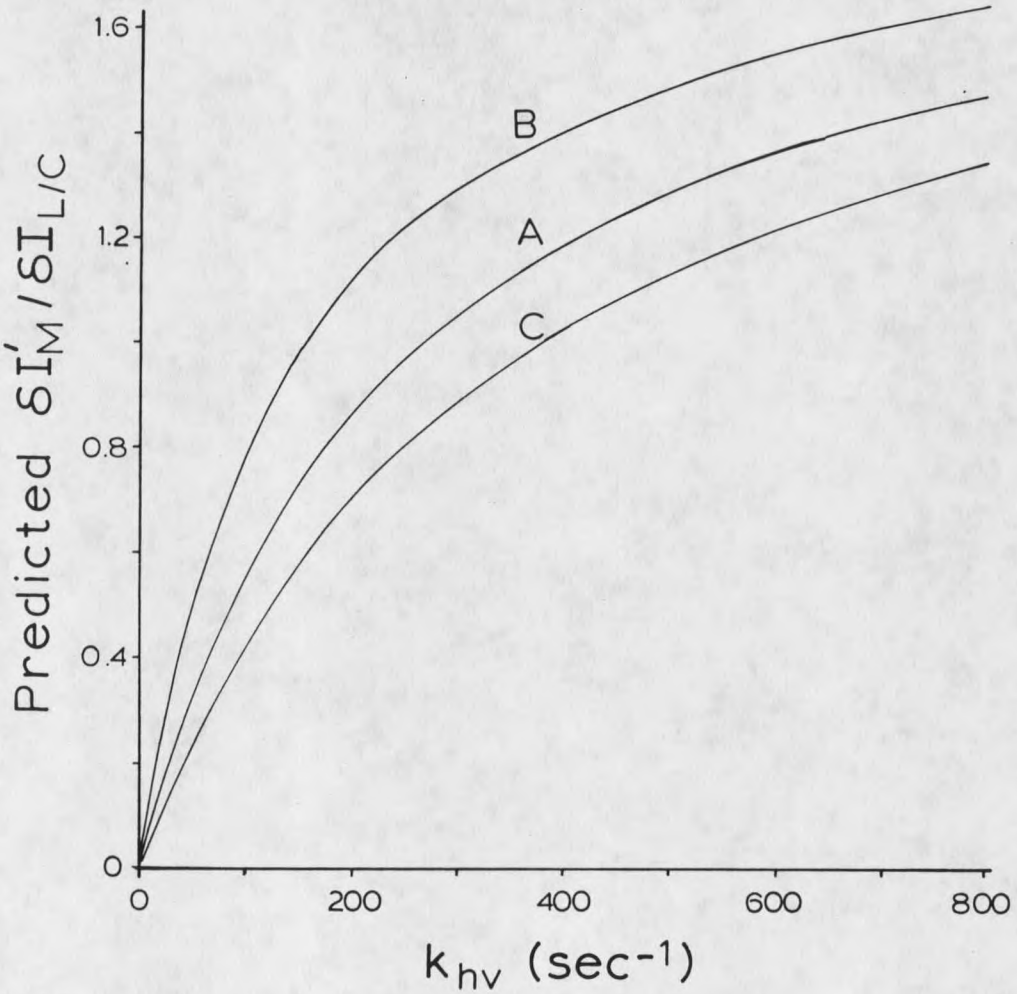

Figure 3. Predicted relationship between the ratio of the $\delta I_{M'}$ and $\delta I_{L/C}$ responses and k_{hv}. Rate coefficients used are those listed in Figure 2 except the values chosen for the negative ion recombination coefficient, $R_{X^-n_+}$, are (A) 100, (B) 50, and (C) 150 s^{-1}.

k_{hv}. The ratio of these two responses is of special interest since it can be obtained simultaneously in an experiment utilizing a chopped light beam. These two responses should also provide a more accurate measure of the processes occurring within the ECD than a comparison of ECD responses with light continuously on or off since bulk heating of the source gas by the intense light (36) can be minimized in a chopped-light experiment. From Figure 3, the ratio of $\delta I_M'$ to $\delta I_{L/C}$ is predicted to be a sensitive function of the rate coefficient, k_{hv}, for Reaction 8. The ratio may provide a means of determining k_{hv} and also σ if Φ can be accurately measured. The accuracy of the method for determining k_{hv} is dependent upon the accuracy of the value for $R_{x^-}n_+$. As described earlier, a value of $R_{x^-}n_+ = 100 \pm 50$ s^{-1} seems reasonable. In Figure 3, curves B and C represent the predicted ratios for $R_{x^-}n_+ = 50$ and 150 s^{-1}, respectively.

EXPERIMENTAL

The experimental setup is shown in Figure 4. The ECD was homebuilt from stainless steel. The ionization chamber is cylindrical, with a length of 2.0 cm and a diameter of 1.2 cm, creating a volume of 2.3 cm^3. A ^{63}Ni-on-Pt foil (New England Nuclear) of 9 mCi activity forms the cylindrical walls of the cell. The anode is a stainless steel pin 1/16 in. in diameter entering the cell from one side through a Teflon plug, and protruding 3 mm into the ionization volume. The ends of the cylindrical cell are formed by fused silica windows which

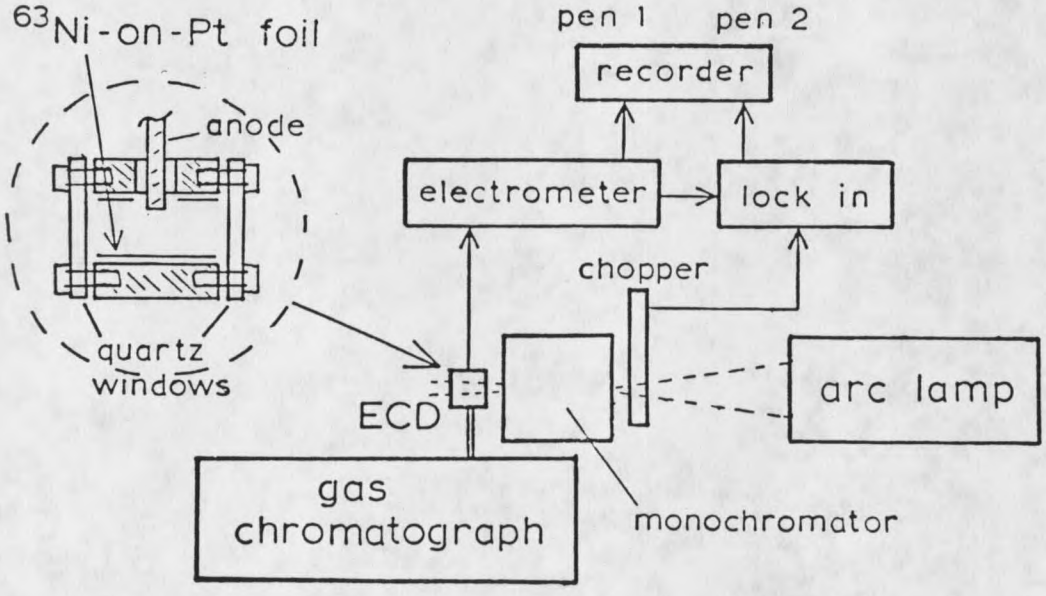

Figure 4. Apparatus used for PD-pulsed ECD measurements.

are sealed with Teflon washers. The cell is heated to 200°C by two cartridge heaters with thermocouple-feedback control. Samples are introduced into the ECD by a gas chromatograph (Varian Model 3700) using one of two combinations of columns and injection methods. For the halocarbons, a 10-ft x 1/8 in. stainless steel column packed with 10% SF-96 on chromosorb W was used. The halocarbons were introduced as gaseous samples using a 5.0 cm^3 gas sampling loop (Carle Model 8030). For the nitroaromatics, a wide-bore 3-meter capillary column (Hewlett-Packard, 50% phenylmethyl silicone stationary phase) was used in conjunction with a heated direct on-column injection port. The effluent of the wide-bore column was mixed with an excess flow of detector make-up gas so that the total gas flow rate was approximately 40 cm^3 min^{-1}. In all cases, the carrier gas and make-up gas were either nitrogen or 10% methane in argon (both from Matheson) and were first passed through water-and oxygen-removing traps (Altech). In order to prevent oxygen from entering the system, a positive pressure of about 100 Torr above atmospheric pressure (630 Torr in Bozeman) was maintained in the ECD by placement of a flow restrictor at the detector gas outlet port. The chromatographic retention times of all compounds studied were known either from previous studies using the same compounds and columns (47) or by parallel analysis of the samples by

GC-MS. The chromatographic data for all compounds used are provided in Appendix B.

The halocarbons were obtained in pure form from commercial suppliers. Mixtures of these in nitrogen gas were prepared by successive dilution into gas-tight glass vessels with final storage in a 4.5 L glass carboy. This carboy was pressurized slightly with nitrogen gas, allowing numerous aliquots to be transferred by 50 cm^3 syringe to the GC sampling loop. The reproducibility of sample delivery is very high (less than 5% variation). The nitroaromatics, quinones, perfluorocarbons, and azulene were also obtained from commercial suppliers and needed no further purification since they were introduced into the ECD with chromatographic separation from impurities, including isomers of the same compound. These aromatic compounds were diluted in either benzene or toluene to an appropriate concentration. Typically, about 0.5 ng of the compound of interest were injected onto the column. Injection sizes were adjusted so as to maintain relatively constant normal ($\delta I_{L/C}$) ECD responses.

All optical components were attached to an optical rail or bench (Edmund Scientific). The optical components consisted of a 1000 W arc lamp (Photon Technology International [PTI], Model A5000), a water filled IR filter (PTI), a mechanical light beam chopper

(PTI, Model 4000), and a single grating monochromator (PTI, Model 01-002), the f/ value being matched to that of the arc lamp. The arc lamp has an elliptical reflector of f/4, which focuses most of the emitted light into a circular image approximately 1 cm in diameter about 43 cm from the front of the lamp housing. The lamp can produce up to 105 W of light power with either the Xe or Hg/Xe lamp. With the Xe lamp, the emission spectrum is relatively evenly spread over the visible and near-UV wavelengths. The Hg/Xe lamp provides greater concentrations of light within certain spectral regions. The emission spectra of both lamps are shown in Figure 1 (page 4). Two different monochromator gratings were used. For the wavelength region of 250-600 nm, a grating with 1200 lines/mm and an optimum wavelength of 400 nm was used. For the spectral region of 600-1200 nm, a grating with 600 lines/mm and an optimum wavelength of 1000 nm was used. The entrance and exit slits of the monochromator were generally set to a width of 5 mm to ensure high light throughput. As a result of these slit widths, the bandwidth of the monochromator was 20 nm for the 1200 lines/mm grating (for λ = 250-600 nm), and 40 nm for the 600 lines/mm grating (for λ = 600-1200 nm). The five-sector disc supplied with the chopper was replaced by a home-built two-sector disc, for which the width of each sector exceeds the size of the light image defined

by either the entrance window of the ECD or the entrance slit of the monochromator by about a factor of 5. This creates an on-off nature of the chopped light beam which closely resembles a square wave with a 50/50 duty cycle.

The signal processing components include the ECD pulser and electrometer (home-built), lock-in amplifier (Princeton Applied Research, Model 5207), two-pen recorder, and light chopper. The basic design of the pulser and electrometer has been described by Grimsrud and Knighton (48). Minor modifications were necessary, primarily in RC time constants. The circuit diagram is shown in Figure 5. The pulser is of the fixed-frequency type and was generally set to a frequency of 2 kHz. With Ar/CH_4 carrier gas, a pulse width of 2 μs was used to collect the electrons. In nitrogen carrier gas, the electrons are less mobile and a pulse width of 10 μs was necessary to collect all of the electrons. The resulting current signal undergoes standard processing (48) by the electrometer circuit and is sent to pen 1 of the recorder and also to the lock-in amplifier. In the lock-in amplifier, the electrometer signal is mixed with the square-wave reference signal from the chopper and sent to pen 2 of the recorder. In a chopped-beam experiment, pen 1 provides a measure of $\delta I_{L/C}$, which, as described in Theory, is closely related to a normal ECD response. Pen 2 simultaneously provides a δI_M response, which is the

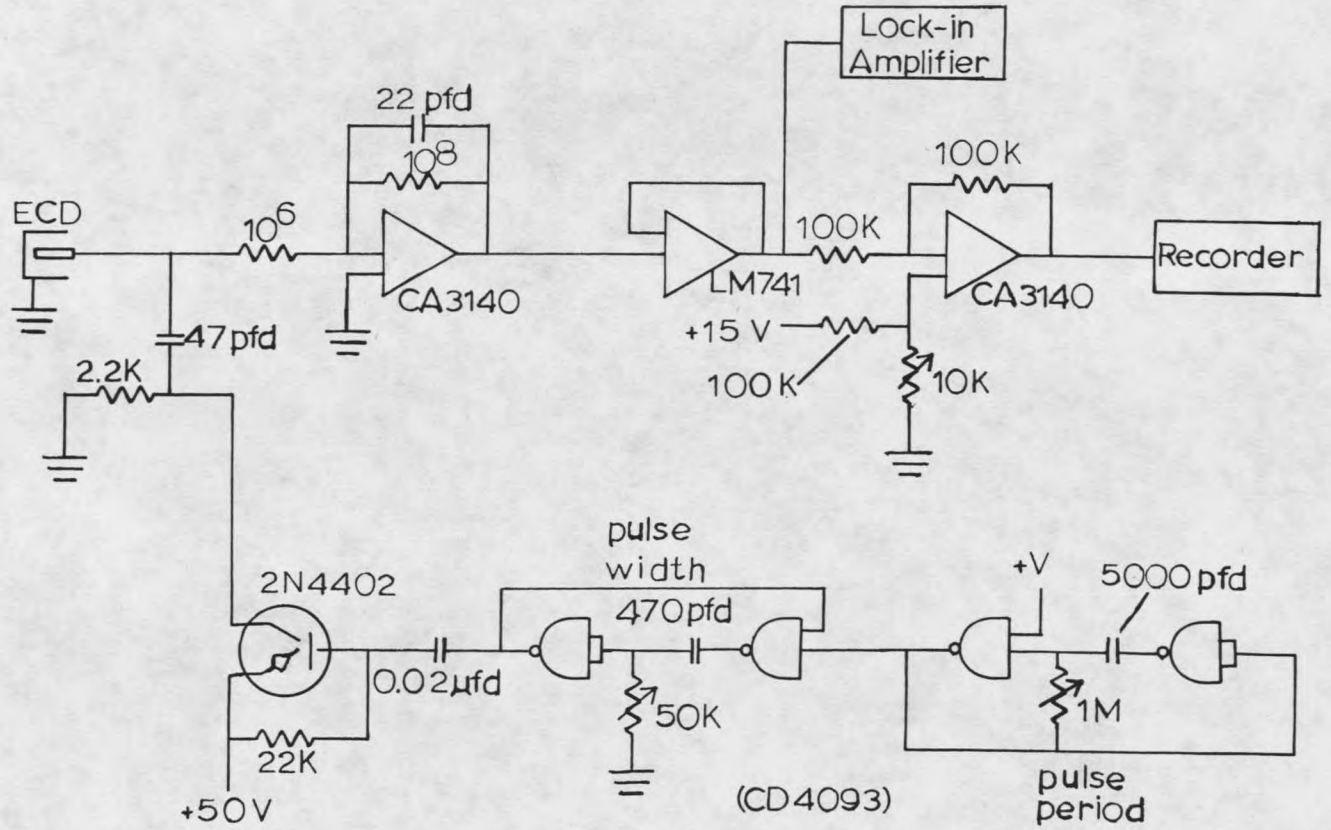

Figure 5. Circuit diagram for the pulser and electrometer used for the PDM-ECD

actual PD-modulated ECD response and is closely related to the $\delta I_M'$ response described in Theory. The relationship between δI_M and $\delta I_M'$ is determined by ECD dynamics and the phase-angle offset of the lock-in amplifier. The other two responses discussed in Theory, δI_N and δI_L, can be provided by pen 1 when the chopper is not used and the light source is either continuously off or on, respectively.

The measurement of relative light flux was obtained by placing one of two instruments immediately behind the exit slit of the monochromator, the place usually occupied by the ECD. For the wavelength range of 250-600 nm, a quantum counter (49) was used. This device is based on the absorption of light by a highly concentrated solution of rhodamine B dye in combination with a photodiode detector. The counter provides a response of constant quantum efficiency to all light in the UV and visible regions with wavelengths shorter than 600 nm. For the wavelength region of 600-1200 nm, relative light power was measured with a volume absorbing disc calorimeter (Scientech, Inc., Model 38-0101). These power measurements were then converted to values of relative light flux (f, photons per second per unit area). A plot of relative photon flux thereby obtained from the Xe lamp over the spectral range used (300-1200 nm) is shown in Figure 6. The variations of flux with

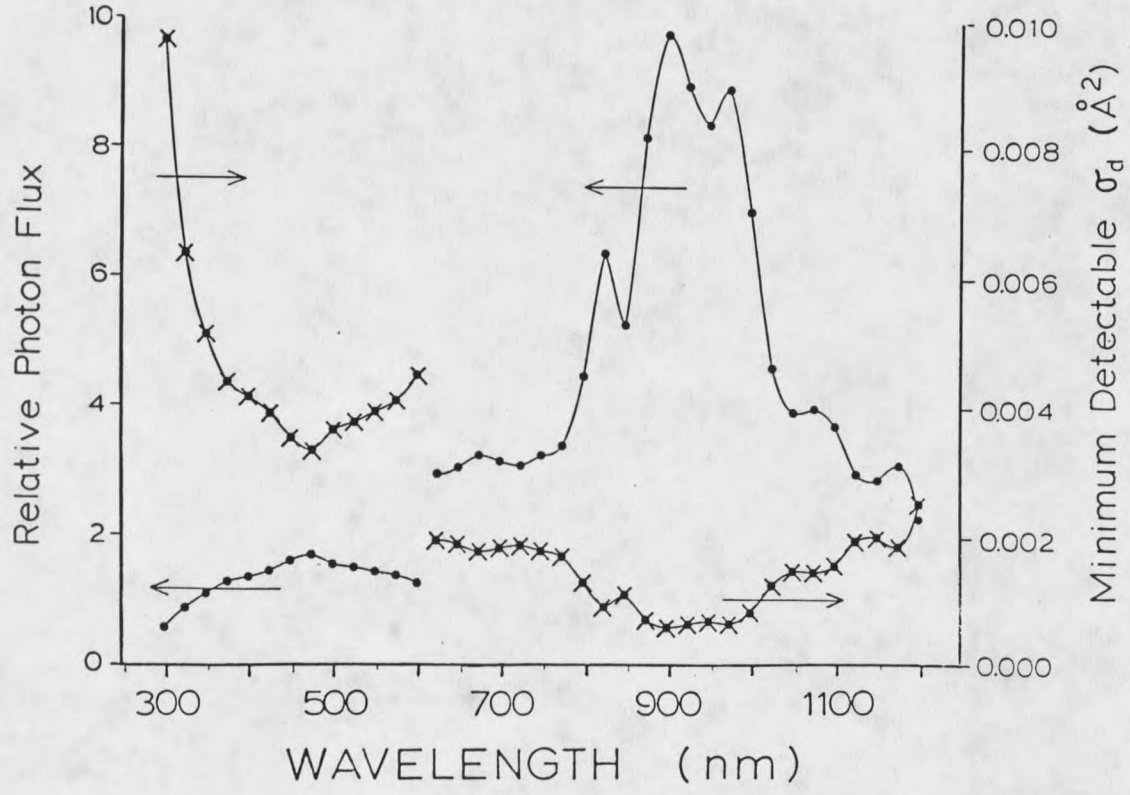

Figure 6. Relative magnitude of light flux (photons per second per unit area) and minimum detectable PD cross-section throughout the spectral range of PD measurements with the Xe lamp. The discontinuity at 600 nm is due to a change in the grating at this wavelength.

wavelength are due to a combination of factors including the spectral emission of the Xe lamp, the monochromator throughput, the change of gratings which occurs at 600 nm, and the use of various cut-off filters which ensure the absence of unwanted light of higher order wavelengths. Also shown in Figure 6 is the minimum

absolute cross-section detectable over the entire spectral range (300-1200 nm), which is inversely related to light intensity.

The measurement of absolute light flux was done with a chemical actinometer (PTI). A fused silica cuvette containing a solution of the cis and trans isomers of azobenzene in methanol was placed behind the exit slit of the monochromator. Both entrance and exit slits were set to a height of 1.0 cm and a width of 0.5 cm. After exposure of this solution to a selected light flux for a specific period of time, the absolute magnitude of the light beam flux (photons s^{-1} cm^{-2}) was calculated, based on the change in absorption of the solution. The absorption measurements were made with a Varian 6345 UV-Vis double beam spectrophotometer. This measurement technique has been described in detail by Zimmerman, Chow, and Paik (50).

In order to simplify the interpretation of the ECD data when obtaining the PD spectrum of a compound, two main conditions were always maintained: 1) the sample size was adjusted so as not to cause more than a 30% change in total standing current, and 2) the light was never intense enough to photodetach more than 20% of the negative ions of interest. To obtain a full PD spectrum of a compound, repeated GC injections were made while varying the wavelength of light selected. A measure of

the relative PD cross-section, rel σ, at each wavelength was obtained from the combination of the PDM-ECD measurements with that of relative light flux, f, shown in Figure 7, in accordance with Equation 9. This

$$\text{rel } \sigma = \delta I_M \; / \; (\delta I_{L/C} \times f) \qquad (9)$$

treatment of the measured responses, δI_M and $\delta I_{L/C}$, with the relative photon flux is thought to be proportional to the PD cross-section. The absolute cross-section for each ion at each wavelength is then determined by comparing the relative σ value to the known absolute cross-section for I^-. The absolute cross-section for I^- was obtained by knowing the absolute light flux and the measured responses. This procedure will be described in detail in Results and Discussion. The measured value for the absolute PD cross-section for I^- was in excellent agreement with the current literature value (13). When the spectra of the halide ions were measured, methyl iodide was included in the sample for cross-section calibration, while for the aromatic molecular anions, 1-iodooctane was included in the sample.

In order to identify the negative ions produced by electron capture, the electron capture mass spectra of all compounds were determined in separate experiments using an atmospheric pressure ionization mass spectrometer (APIMS). This instrument is also home-built

(38) and includes a ^{63}Ni-based ion source where conditions can be made essentially identical to those existing within the PDM-ECD. These measurements were carried out with capillary GC introduction to the APIMS ion source, which was maintained at the same temperature as the ECD (usually 200°C).

RESULTS AND DISCUSSION

The Results and Discussion chapter is divided into ten parts. The first two parts deal with the development and characterization of the experimental system. The third part describes the determination of the PD spectra and measurements of absolute cross-sections for the halide anions. Part four deals with the application of the PDM-ECD system for chemical analysis. Parts five through seven describe the PD spectra of molecular anions, particularly the nitroaromatic anions, and addresses the interpretation of their spectra. Parts eight and nine describe the application of the PDM-ECD to kinetic studies, measuring an electron autodetachment rate for azulene and the EC chemistry of $CBrCl_3$, respectively. Part ten is a short section discussing the location of negative ions in the ECD.

General Characterization of the PDM-ECD

Characterization of PD Response Perturbations

The compounds chosen for study in this initial phase of the project were various halogenated hydrocarbons which are known to produce I^-, Br^-, or Cl^- upon electron capture. These anions are commonly produced in ECD

analyses, so the results would be applicable to environmental sampling. Also, the photodetachment spectra of the halides have been previously reported in the literature (13-15, 17), allowing the comparison of the experimental results with theoretically predicted responses.

In order to characterize the PD perturbation of the responses for the halide anions, initial measurements were made using the full light emission of the Xe lamp. Figure 7 shows a series of chromatograms taken with the full lamp emission, where no monochromator or filters were used. The chromatogram in column A was obtained with the Xe lamp set at approximately 40% power. This power setting was chosen since, without any filtering or wavelength selecting device in the light beam, higher power settings tended to create more heating and electronic noise problems. The compounds present in the chromatograms of column A are CF_2Br_2, CH_3I, $CHCl_3$, and CCl_4 which produce Br^-, I^-, Cl^-, and Cl^-, respectively, upon electron capture (40). The first (top) chromatogram in column A was obtained with the light off and provides the normal ECD response, δI_N. The sample sizes chosen create normal responses which do not exceed approximately 10% of the ECD standing current (about 3.5 nA).

The second chromatogram in column A was obtained with the light beam continuously passed through the ECD.

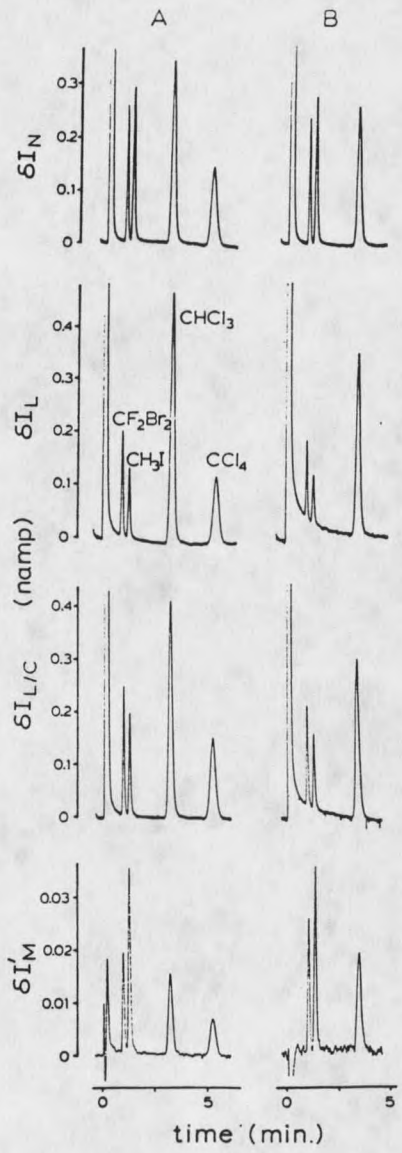

Figure 7. Chromatograms obtained from analysis using the four different response functions possible using light in the ECD. Chromatograms in column A were obtained with the full emission of a Xe lamp (40 % power); those in column B with the full emission from a Hg/Xe lamp (40 % power). The response functions shown were obtained with: (1) light off, (2) light always on, (3) and a chopped (43 Hz) light beam. (4) Obtained simultaneously with response 3 by amplification of the modulated ECD signal.

The ECD response to CH_3I is reduced to a magnitude 0.45 as great as the light off response, δI_N. The responses to CF_2Br_2 and CCl_4 are also reduced to magnitudes 0.67 and 0.85, respectively, as great as their δI_N responses. These effects are consistent with Figure 1 (page 4) which shows the PD cross-section for I^-, Br^-, and Cl^-, as well as the emission spectra of the Xe and Hg/Xe lamps. The cross-section data is reproduced from papers by Mandl (13, 14). The figure indicates that the rates of PD with the Xe lamp should be greatest for I^-, less for Br^-, and smallest for Cl^-. As was shown in Figure 3, PD effects as large as those observed in Figure 7 could be expected for ions with large cross-sections irradiated with intense light. In the δI_L response measurements, it was estimated that between 2 and 4 W of light between 250 and 400 nm were passing through the ECD. From Figure 1, it is clear that the σ values for the three halides listed are large in this wavelength region. Therefore, the observed effects are in good qualitative agreement with expected responses, and the differences between the δI_N and δI_L responses can be attributed primarily to PD.

The magnitudes of the δI_L and δI_N responses to $CHCl_3$ require additional explanation. For $CHCl_3$, the ECD response has been increased by a factor of 1.35 by the same light flux which decreased the responses to the other three halocarbons. This increased response is

thought to be caused by an increase in temperature of the ECD gas when the high intensity light is used. The electron capture coefficient for $CHCl_3$ is much smaller and more temperature dependent than for the other compounds present (40). With the light on, then, the increased rate of Reaction 6, electron capture, for $CHCl_3$ exceeds the rate of PD of Cl^-, Reaction 8. It will be shown later that this heating effect is minimized or eliminated when the light beam is chopped. This unwanted response characteristic for $CHCl_3$ raises the question as to what effects the continuous light exposure might also have on other compounds and their responses. As was also concluded by Dovichi and Keller (36), use of a light beam chopper and lock-in amplifier is generally a superior method for measuring PD in the ECD.

The third and fourth chromatograms in column A of Figure 7 were obtained simultaneously while the light beam was chopped at a frequency of 43 Hz. The $\delta I_{L/C}$ responses, the third chromatogram, were obtained directly from the electrometer, and are clearly intermediate in magnitude between the δI_N and δI_L responses as predicted in Theory. The magnitude of the $\delta I_{L/C}$ responses to all compounds was found to be independent of chopping frequency.

The fourth chromatogram in column A of Figure 7 is the PD-modulated response, δI_M, obtained from the lock-in

amplifier. This chromatogram reveals several important aspects of the modulated experiment. First, this chromatogram shows that, in fact, PDM-ECD responses can be measured with good signal-to-noise characteristics by the lock-in amplifier. Also, the PD-modulated response to $CHCl_3$ is of the same sign as the other compounds even though its SI_L response was greater than δI_N. A comparison of the $CHCl_3$ and CCl_4 responses in the third and fourth chromatograms in column A will, in fact, indicate that their $\delta I_M/\delta I_{L/C}$ ratios are nearly identical. This indicates that the previously discussed thermal effect for $CHCl_3$ is not important when the light is chopped, and that the PD of Cl^- is dominating the δI_M responses for both $CHCl_3$ and CCl_4.

A comparison of the relative magnitudes of the PD-modulated responses for the Cl^-, Br^-, and I^- generating molecules is made in Figure 8. Here, a series of analyses was made on the sample mixture at various levels of light intensity from the Xe lamp. In the figure, the ratios of the δI_M to $\delta I_{L/C}$ responses observed for CH_3I, CF_2Br_2, and CCl_4 are shown as a function of the measured relative light intensity. The ratio of responses is a very useful means of characterizing PD responses, since the ratio is independent of sample concentration (as long as the normal ECD response does not exceed approximately 30% of the total ECD standing

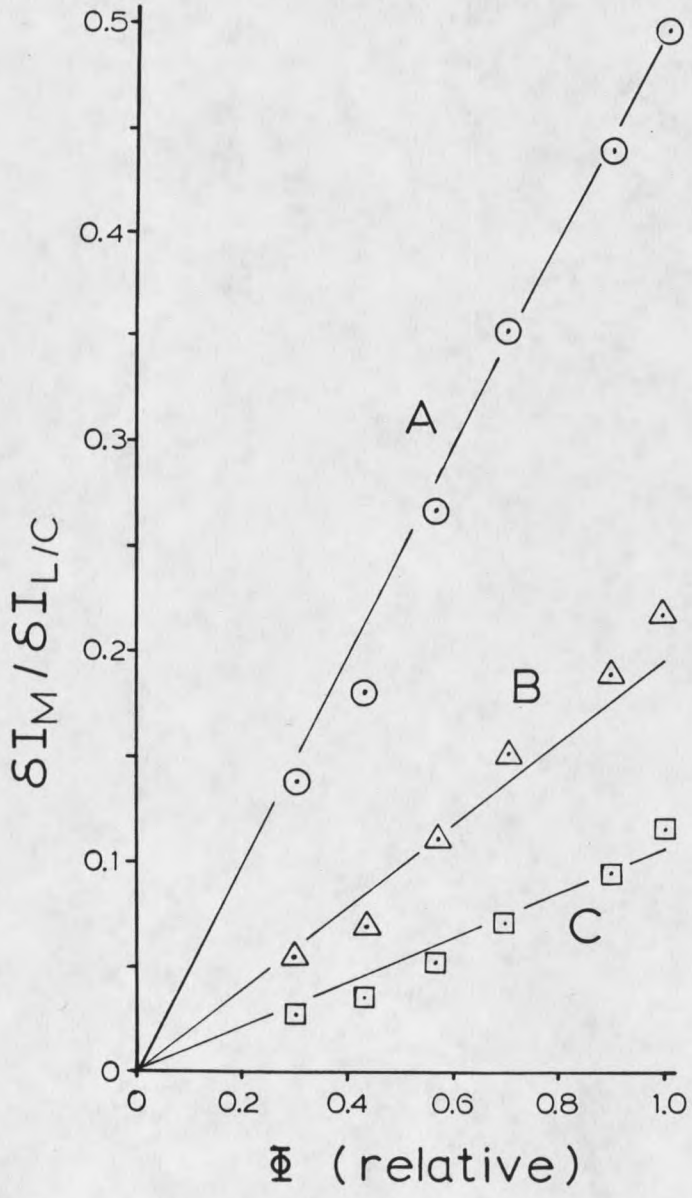

Figure 8. Ratio of $\delta I_M/\delta I_{L/C}$ responses to (A) CH_3I, (B) CF_2Br_2, and (C) $CHCl_3$ observed with use of various relative intensities of light emitted by the Xe arc lamp, without use of a monochromator or filters. Solid lines are predictions of relative response ratios based on the overlap integrals of the PD cross-sections and the Xe lamp emission spectrum shown in Figure 1.

current). Figure 8 indicates that these response ratios are directly proportional to light intensity and, with all intensities of light used, have nearly the following relative average values: 1.0 for CH_3I, 0.45 for CF_2Br_2, and 0.23 for CCl_4. The solid lines in Figure 8 are predictions of relative responses and have been obtained from the relative overlap integrals of the PD cross-sections for I^-, Br^-, and Cl^- and the relative emission spectrum for the Xe lamp, both of which are shown in Figure 1. The relative magnitudes of the overlap integrals are 1.00 for I^-, 0.39 for Br^-, and 0.21 for Cl^-. Line A in Figure 8 was arbitrarily set to best fit the CH_3I data. The excellent agreement between the solid lines and the data points for CF_2Br_2 and $CHCl_3$ in Figure 8 provides strong evidence that the interpretation of the modulated signals is valid and consistent.

In column B of Figure 7, the corresponding chromatograms, without CCl_4, have been obtained using the Hg/Xe lamp, again at about 40% power. This lamp should provide a greater fraction of its total power in the 250-400 nm range than does the Xe lamp, and larger PD responses are, in fact, observed. In comparing the relative PD-modulated responses in the last two chromatograms in columns A and B in Figure 7, it is seen that the δI_M responses to the Br^- and Cl^- producing molecules have increased somewhat more by the change to

the Hg/Xe lamp than the modulated response to CH_3I. This can again be explained in terms of the overlap integrals of the cross-sections and the Hg/Xe emission spectrum shown in Figure 1. The relative overlap integrals are 1.00, 0.51, and 0.32 for I^-, Br^-, and Cl^-, respectively. These ratios predict slightly higher responses for Cl^- and Br^- relative to that of I^- than did the corresponding overlap integrals for the Xe lamps (1.00, 0.39, 0.21) discussed previously.

Effect of Chopping Frequency on PDM-ECD Responses

Figure 9 shows that the magnitude of the δI_M responses observed for all compounds is dependent upon the frequency of the light beam chopper. Figure 9 also shows that the phase angle offset (automatically selected by the lock-in amplifier in order to maximize the modulated output signal) is also dependent upon the chopping frequency. At slow chopping frequencies, 13-20 Hz, the δI_M responses are largest and the phase angle offset is nearly zero degrees. As the chopping frequency is increased, the magnitude of the δI_M response decreases and the optimum phase angle changes from 0° to -90°. The dependencies of the δI_M response and the phase angle are independent of sample size, light intensity, and ECD pulsing frequency.

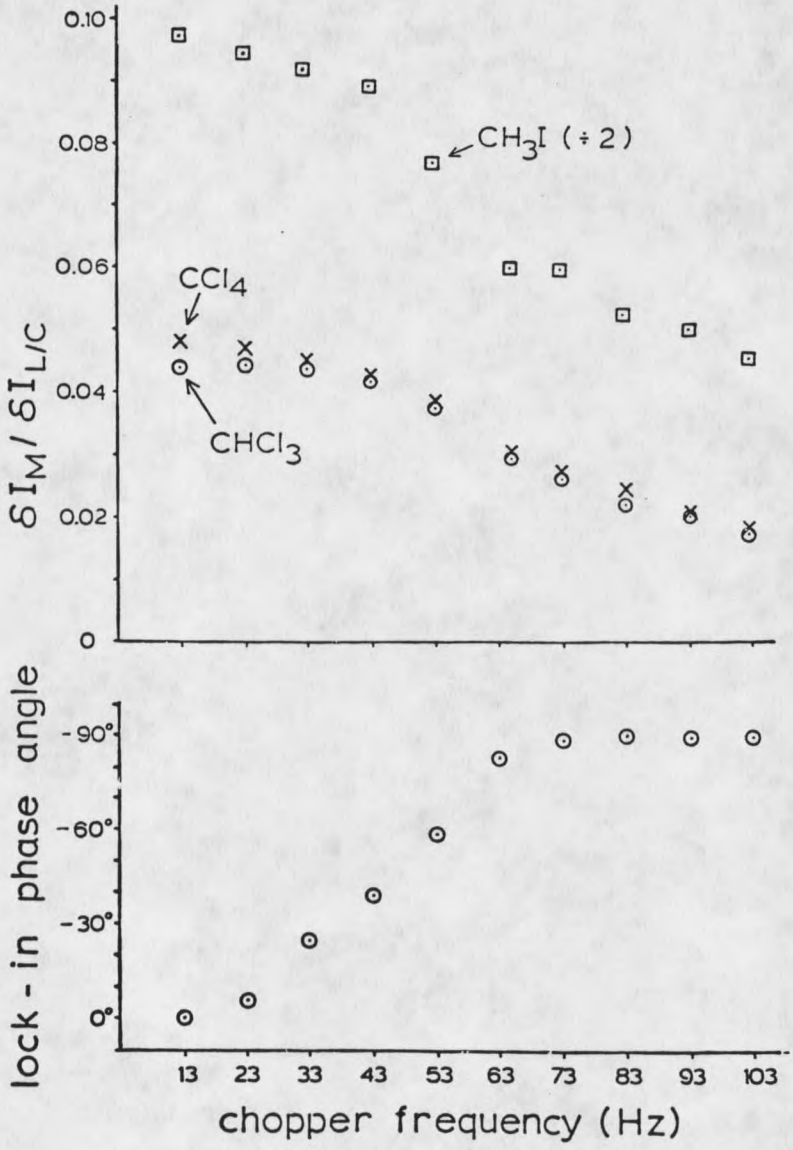

Figure 9. Observed δI_M / $\delta I_{L/C}$ response ratios and phase angle offsets in the chromatographic analysis of CH_3I, $CHCl_3$, and CCl_4 as a function of chopper frequency.

Figure 10, which shows the two waveforms sent to the lock-in amplifier, will be useful in explaining the frequency dependence of the responses. The square wave is the signal received from the chopper, and the other waveform is that received from the ECD electrometer. The four cases shown represent progressively faster chopping frequencies. If the chopping frequency is slow with respect to the time required for the ECD to establish the light-on and light-off steady-state conditions, the signal waveform received from the ECD electrometer will closely resemble a square wave, shown as case A in Figure 10. If the frequency of chopping is made more rapid, the chemical dynamics of the ECD will continuously lag behind the light pulses by an increasing margin, as shown in case B, until the situation shown as case C is reached, where the dynamics of the ECD are moderateley slow on the time scale established by the light beam chopper and the signal waveform becomes triangular. Any further increase in chopping frequency continues to produce a triangular waveform, but of smaller amplitude, shown as case D. Also illustrated in Figure 10 is the phase angle that would be automatically selected by the lock-in amplifier in order to maximize the modulated output signal. This phase angle is expected to vary from 0° to -90° as chopping is changed from a slow to a fast frequency. The magnitude of the lock-in amplifier output expected for

each case shown in Figure 10 is qualitatively indicated by the shaded areas under the signal waveforms. As was experimentally observed in Figure 9, a decrease in the modulated response is predicted with increased chopping frequency.

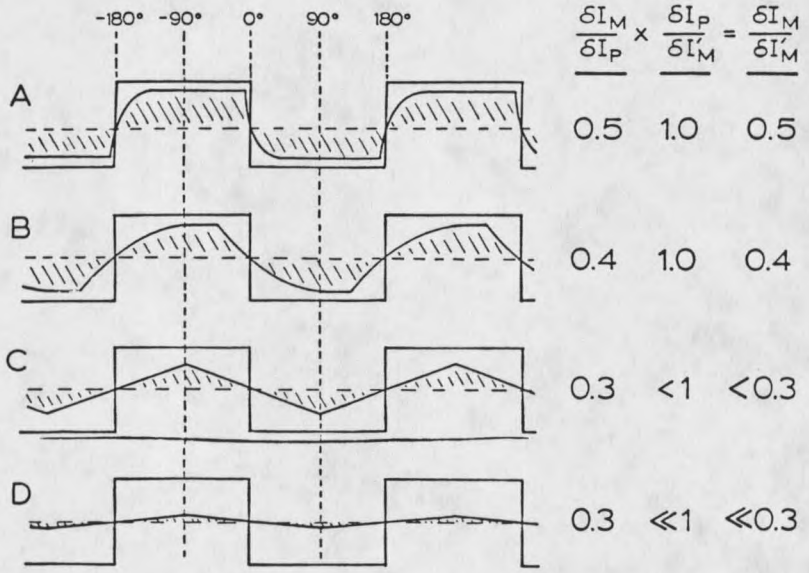

Figure 10. Simulations of the two waveforms sent to the lock-in amplifier and the phase angle offset selected by the lock-in amplifier in order to provide a maximized output signal. For the four cases shown, the frequency of the true square wave, which is received from the light beam chopper, increases continuously in the order A, B, C, D. The other waveform shown is that received from the electrometer and assumes a shape determined by the dynamics of the ECD and the frequency of the chopper. These simulations are used to explain the observed variations of the phase angle offsets and δI_M responses with changes in chopping frequency.

The relationship between δI_M, the phase angle, and the chopping frequency is quantitatively analogous to that expected when a square wave is passed through a low-pass electronic filter (51). The fractional attenuation of the δI_M signal, α, which is observed with higher chopping frequencies, f, will be given by Equation 9, where t is the time constant for the rate of change

$$\alpha = (1+(2\pi ft)^2)^{-\frac{1}{2}} \qquad (9)$$

of the chemical system within the ECD. Also, the phase angle, θ, will be given by Equation 10. Fitting either of these equations to the data in Figure 9 yields the

$$\text{Tan } \theta = 1 \; / \; 2\pi ft \qquad (10)$$

result that $t \approx 3.5$ ms (for example, with f = 45 Hz, Figure 9 indicates that $\theta = 45°$, and Tan 45° = 1 / 2πt(45 Hz) leads to t = 3.5 ms). Since the magnitude of t is independent of sample size and light intensity, the chemical process which provides the rate-limiting step does not appear to be Reaction 6, 7, or 8. Computer simulations suggest that the rate limiting process is Reaction 5, the electron-ion recombination reaction. As stated in Theory, measurements by an independent method have shown that the first order rate constant for Reaction 5 is $R_e n_+ = 300\ s^{-1}$. The time constant associated with electron loss by Reaction 5 is,

therefore, 3.3 ms and is essentially identical to the value of t indicated by the data in Figure 9. This evidence strongly suggests that Reaction 5 is the process which determines the response dependencies observed with chopping frequency.

With this information from Figures 9 and 10, it is now possible to extract $\delta I_M'$, the form of the PDM-ECD response developed in Theory, from the chopped beam experiments. The attenuation of the observed PD-modulated response with increased chopping frequency is one of two factors which must be considered. The second factor is that the lock-in amplifier provides a direct current (DC) output equal to the root mean square (rms) power of the signal waveform. The $\delta I_M'$ response, however, as it was defined in Theory, is the peak-to-peak difference in the PD-modulated signal. Therefore, a factor of 0.5 (51) must also be included in the conversion of δI_M to $\delta I_M'$. The full equation which then applies to the measurements is shown as Equation 11,

$$\delta I_M = 0.5\ \alpha \times \delta I_M' = 0.5\ (1+(2\pi ft)^2)^{-\frac{1}{2}} \times \delta I_M' \qquad (11)$$

where t = 3.5 ms. The absolute magnitudes of the various δI responses shown in Figure 7 can now be more completely understood. For example, a δI_M measurement of 0.020 nA was obtained for CF_2Br_2 in column A of Figure 7 with a chopping frequency of 43 Hz, while the difference

in the δI_N and δI_L responses was 0.060 nA. According to the predictions shown in Figure 2, $\delta I_M'$ should be equal to the difference between δI_N and δI_L. At this chopping frequency (43 Hz), the equation given above provides the following relationship between the observed and predicted responses: $\delta I_M = 0.36 \times \delta I_M'$. Thus, $\delta I_M' = 0.020$ nA/0.36 = 0.056 nA is obtained for CF_2Br_2. This calculation is now in satisfactory agreement with the measured $\delta I_N - \delta I_L$ difference of 0.060 nA. Any remaining discrepancy may be attributable to heating effects in the δI_L experiments.

Measurement of PD Spectra of the Halide Anions

If the PDM-ECD is responding to only PD of the negative ions formed by electron capture, the PDM-ECD measurements should be in agreement with the known PD spectra of these negative ions determined by more established techniques. With a monochromator and selected 20 nm bandwidths of light emitted by the Xe lamp, the PDM-ECD responses to CF_2Br_2, CH_3I, and $CHCl_3$ shown in Figure 11 were obtained. With the monochromator set to 330 nm, PD-modulated responses for all three compounds are observed. With 365 nm light, the modulated response to $CHCl_3$ is eliminated. With 395 nm light, only a response to CH_3I is observed. At 425 nm, no modulated responses to any of the three compounds are observed. This is in qualitative agreement with literature

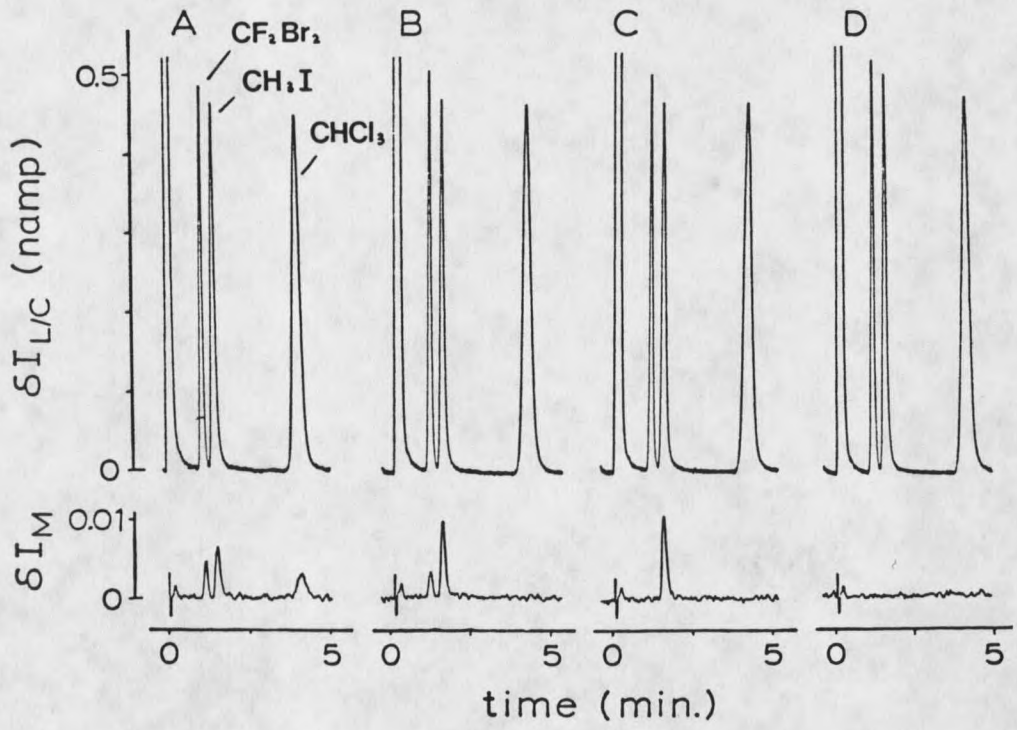

Figure 11. $\delta I_{L/C}$ and δI_M responses simultaneously observed in the repeated analysis of a sample containing CF_2Br_2, CH_3I, and $CHCl_3$. Along with the Xe arc lamp, a monochromator has been used and set to (A) 330 nm, (B) 365 nm, (C) 395 nm, (D) 425 nm.

photodetachment cross-sections shown in Figure 1.

PD measurements were also obtained over a range of selected wavelengths along with measurements of relative light flux obtained with a quantum counter. In Figure 12 this data has been plotted in a form which is expected to be proportional to the photodetachment cross-sections at each wavelength. A comparison of the PD spectra thereby obtained for I^-, Br^-, and Cl^- in Figure 12 with those of Mandl (8, 9) shown in Figure 1 indicates a high level of agreement. The major difference is that the onsets for PD obtained by the PDM-ECD method are not as sharp as those of Mandl (8, 9), which is undoubtedly due to the use of a relatively broad bandpass of light in the PDM-ECD experiments.

Measurement of an Absolute PD Cross-section for Iodide

By combining measurements of absolute light flux with PDM-ECD measurements, it should be possible to obtain absolute PD cross-sections for any negative ion of interest. A determination of this type was done for I^-. With the Xe lamp set at three different power levels and the monochromator set to 365 nm, nine determinations of the absolute cross-section for I^- were made. The magnitude of the light flux was measured by a chemical actinometer, as described in Experimental. The PDM-ECD response to CH_3I along with the $\delta I_{L/C}$ response was then

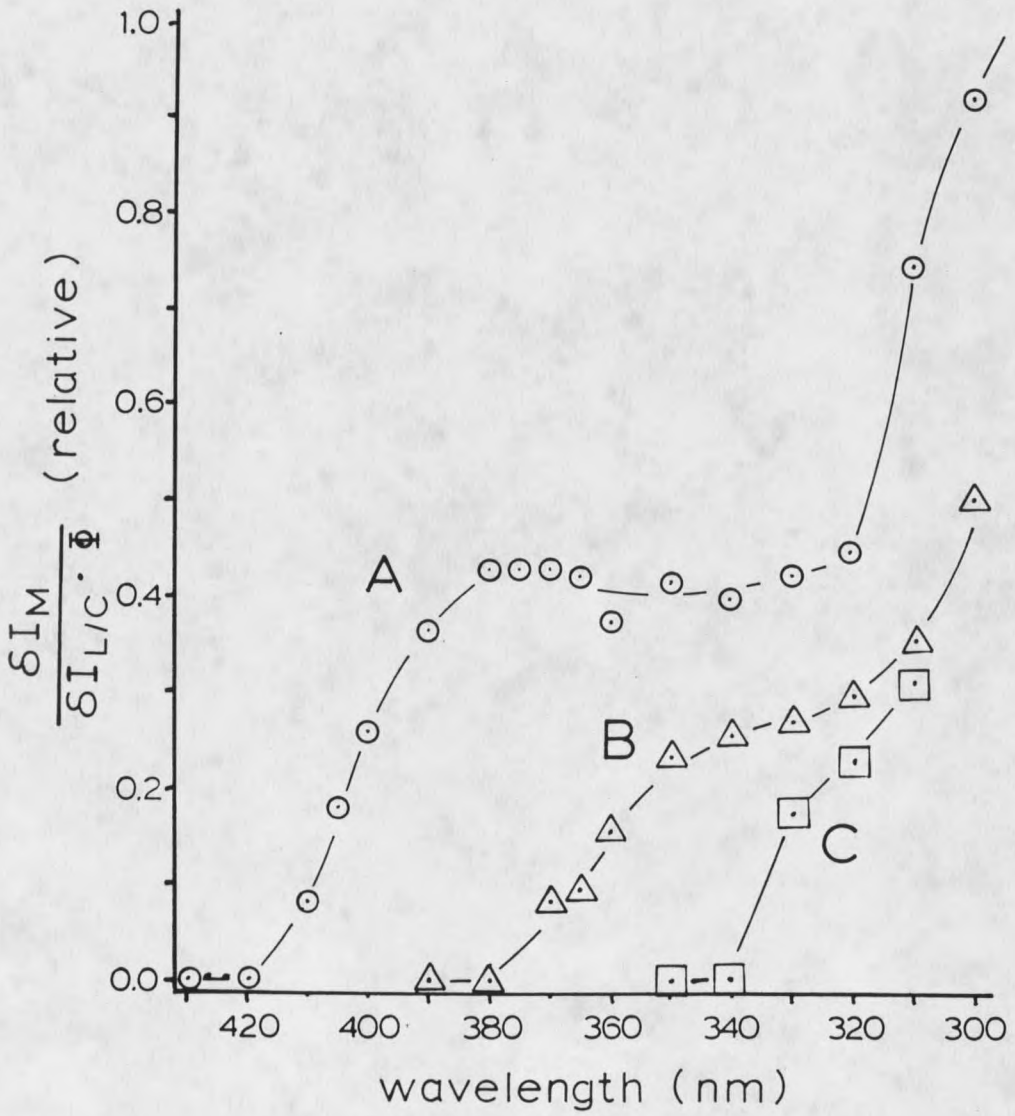

Figure 12. Measured PD spectra of (A) iodide, (B) bromide, and (C) chloride. δI_M and $\delta I_{L/C}$ response ratios observed for CH_3I, CF_2Br_2, and $CHCl_3$ and measured relative light flux, Φ, are plotted in a functional form that is expected to be proportional to the PD cross-sections at each wavelength.

measured three times at each power setting of the arc lamp using a chopping frequency of 43 Hz. As described previously, a value for $\delta I_M'$ is obtained from the raw δI_M responses shown for each case by division by 0.36, the appropriate correction factor for f = 43 Hz. The rate coefficient for PD, k_{hv}, is then calculated from Equation 12. This equation describes the relationship between the

$$k_{hv}\ (s^{-1}) = 185 \times (\delta I_M'/\delta I_{L/C}) \qquad (12)$$

predicted response ratios and k_{hv} over the initial linear portion of curve A in Figure 3, where the response ratios are less than about 0.2 (185 is the slope of the linear portion). The PD cross-section is then obtained for each individual measurement using Equation 13.

$$\sigma = k_{hv}/\Phi \qquad (13)$$

The nine determinations for the PD cross-section for I^- at 365 nm, shown in Table 1, are in excellent agreement with each other. The average of the values is $\sigma = 2.2 \times 10^{-17}$ cm² with a standard deviation of 0.2×10^{-17} cm². The greatest source of uncertainty is thought to lie not with the experimental measurements, but in the conversion of the response ratios, $\delta I_M'/\delta I_{L/C}$, to a value for k_{hv}. As discussed in Theory, the estimated uncertainty of this conversion is thought to be about ±50%. Therefore, the determination of σ for I^- and its

Expt#	[a] Lamp Power (Watts)	[b] Φ $\left(\frac{\text{Photons}}{\text{cm}^2}\right)$	$\delta I_{L/C}$ (pA)	[c] δI_M (pA)	[d] $\delta I_M'$ (pA)	$\delta I_M'/\delta I_{L/C}$	[e] $k_{h\nu}(\text{sec}^{-1})$	[f] $\sigma(\text{cm})^2$
1	1000	5.7×10^{17}	300	7.5	18.8	0.062	11.5	2.0×10^{-17}
2	"	"	303	6.8	17.0	0.056	10.4	1.8×10^{-17}
3	"	"	308	6.5	16.3	0.053	9.8	1.7×10^{-17}
4	800	3.0×10^{17}	318	4.5	11.3	0.035	6.5	2.2×10^{-17}
5	"	"	310	4.5	11.3	0.036	6.7	2.2×10^{-17}
6	"	"	290	4.0	10.0	0.035	6.5	2.2×10^{-17}
7	640	2.2×10^{17}	310	3.2	8.0	0.026	4.8	2.2×10^{-17}
8	"	"	320	3.0	7.5	0.023	4.3	2.0×10^{-17}
9	"	"	301	3.0	7.5	0.025	4.6	2.1×10^{-17}
							$\sigma_{ave} = 2.03 \times 10^{-17}$	
							st.dev. $= 0.20 \times 10^{-17}$	

[a] Xenon arc lamp used with monochromator set to 365 nm.

[b] Absolute light intensity measured by chemical actinometer. Average of seven measurements at each lamp power setting. Uncertainty of measurements is ±20% at 90% confidence level.

[c] PDM-ECD response measured with chopping frequency of 43 Hz.

[d] Calculated from the measured δI_M response by: $\delta I_M' = \delta I_M/0.40$.

[e] Calculated from: $k_{h\nu}(\text{sec}^{-1}) = 185\ (\delta I_M'/\delta I_{L/C})$

[f] Calculated from: $\sigma = k_{h\nu}/\Phi$

Table 1. Determination of the absolute photodetachment cross-section for iodide by PDM-ECD measurements at 365 nm.

associated uncertainty is $\sigma = 2.2 \pm 1.0 \times 10^{-17}$ cm^2. This result is in good agreement with the results of Mandl (13), shown in Figure 1, who reported a value of $1.9 \pm 0.5 \times 10^{-17}$ cm^2 for I^- at 365 nm. This successful measurement of an absolute PD cross-section by the PDM-ECD is additional strong support for the validity of the model described in Theory.

Application of the PDM-ECD to Chemical Analysis

Use of PDM-ECD Responses for Chemical Analysis

From the results described in previous sections, and particularly from those shown in Figure 11, it appears that the PDM-ECD should be useful for increasing the response specificity of the ECD. For the mixture of halocarbons analyzed in Figure 11, it was shown that a detector which responds only to I^-, to I^- and Br^-, to I^-, Br^-, and Cl^-, or to none of these can be created simply by adjusting a monochromator dial. Furthermore, any of these detection modes can be obtained simultaneously with the $\delta I_{L/C}$ response function, which closely resembles the normal ECD detection mode. The magnitudes of both the δI_M and $\delta I_{L/C}$ responses to the compounds studied here have been found to vary linearly with sample concentration (with a zero intercept) throughout the normal linear range of the pulsed ECD.

In the Introduction, the need for additional degrees of response specificity in the analysis by the ECD of complex mixtures was described. Figure 13 provides an illustration of how the PDM-ECD can add some specificity to analysis. The sample analyzed contains a mixture of eleven halocarbons, some of which are coeluting compounds making the quantitative determination of four of the compounds impossible by normal ECD detection with this column. In order to obtain the lower chromatogram in Figure 13, the intense emission at 365 nm of the Hg/Xe lamp (see Figure 1) operated at full power was selected. To further increase the light intensity within the cell, an aluminum mirror was placed behind the exit window of the ECD. At 365 nm, no PDM responses to the compounds which undergo electron capture to produce Cl^- are expected, while strong responses to I^- and Br^- producing compounds are. Furthermore, from Figure 12, the expected $\delta I_M/\delta I_{L/C}$ response ratios for the iodides should be about 3 times greater than for the bromides, and this is, in fact, observed in Figure 13.

The lower chromatogram in Figure 13 is much simpler, since responses only to the iodides and bromides are provided, and no detectable PDM responses to the chlorides are observed. Along with standard calibration procedures, the lower chromatogram provides a means of independently determining the amounts of CF_2Br_2 and

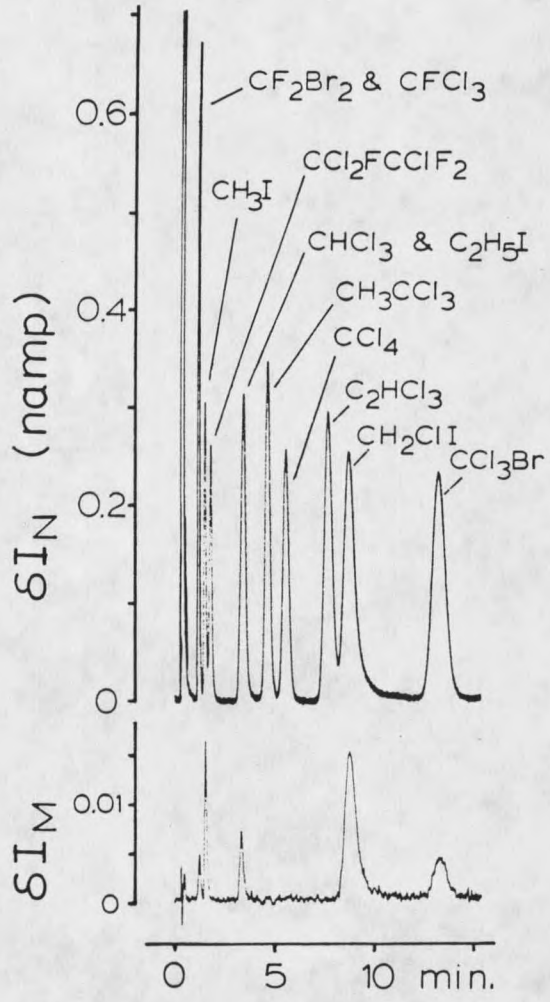

Figure 13. Chromatographic analysis of a mixture of 11 halogenated hydrocarbons with simultaneous detection by the $\delta I_{L/C}$ and δI_M modes of the PDM-pulsed ECD. The top chromatogram provides responses to all compounds present, while the lower chromatogram provides responses only to the bromides and iodides. 365 nm light from a Hg/Xe arc lamp is used. The concentrations of the halocarbons, in the order shown in the upper chromatogram, are: 1.3, 2.0, 0.6, 25, 8.5, 10, 19, 2.4, 900, 3.3, and 15 ppb in nitrogen.

C_2H_5I present, compounds which coelute with $CFCl_3$ and $CHCl_3$, respectively. Quantitative analysis of the latter two chlorine-containing compounds is then possible by subtraction of the bromide and iodide contributions from the $\delta I_{L/C}$ responses. The contributions of CF_2Br_2 and C_2H_5I to the mixed $\delta I_{L/C}$ peaks can be deduced from either their calibrated $\delta I_{L/C}$ responses or by their calibrated δI_M responses along with knowledge of the $\delta I_M/\delta I_{L/C}$ response ratios expected for the bromides and iodides. These ratios are easily determined under a given set of conditions and are available from the responses of the other bromides and iodides shown in Figure 13 which elute as single-component peaks.

The cases of CH_2ClI and $CBrCl_3$ in Figure 13 warrant special attention since it is conceivable that both I^- and Cl^-, for the first molecule, and Br^- and Cl^-, for the second, could have been produced from their EC reactions. From the $\delta I_M/\delta I_{L/C}$ ratios, it can be deduced that only I^- in the first case, and mainly Br^- for the second, are produced. For CH_2ClI, the response ratio is 0.135, while that for CH_3I, which can produce only I^-, is nearly identical, 0.131. For CCl_3Br, the response ratio is 0.033, while for CF_2Br_2, which produces only Br^-, the ratio is 0.037 under identical experimental conditions. This suggests that mainly Br^- and possibly a small amount

of Cl^- are produced in EC by CCl_3Br under these experimental conditions. This is consistent with mass spectral measurements of the EC reactions of CCl_3Br in which a Br^- to Cl^- abundance ratio of about 4 to 1 was observed (52). However, the apparent branching ratio was found to vary somewhat under different experimental conditions. The EC branching ratio of CCl_3Br and also possible secondary EC reactions observed for the EC products of CCl_3Br will be addressed in greater detail in a later section.

Detection Limits of the PDM-ECD

As with any method for trace analysis, it is important to determine the detection limits which might be attained. While the PDM-ECD system has not yet been perfected with respect to optimal signal-to-noise responses, the currently attainable detection limit will be described. Figure 14 shows the signal-to-noise characteristics, and therefore the detection limits, for the same electrometer used under normal ECD conditions and also for the PDM-ECD experiment. The 5 cm^3 nitrogen samples contained 70 pptr CH_3I, 4.5 ppb $CHCl_3$, and 300 pptr CCl_4. The top chromatogram was obtained by the conventional ECD mode with the lamp off, and the second and third chromatograms were obtained simultaneously with a Hg/Xe chopped light beam of 365 nm. With the same

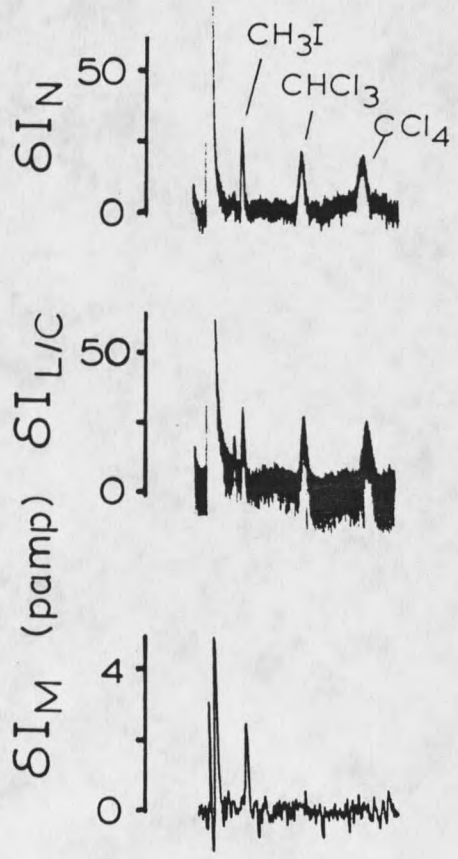

Figure 14. Two repeated analyses of a 5 cm^3 nitrogen gas sample containing 70 pptr CH_3I, 4.5 ppb $CHCl_3$, and 300 pptr CCl_4. For the first analysis, the normal δI_N mode of pulsed ECD detection was used with the arc lamp turned off. In the second analysis, the lower two chromatograms were simultaneously obtained by the $\delta I_{L/C}$ and δI_M modes of PDM-ECD detection with 365 nm light from the Hg/Xe arc lamp.

electrometer, the signal-to-noise ratio of the response to CH_3I obtained in the PDM mode is about the same as that obtained in the normal ECD mode. In both cases, a detection limit of about 10 parts per trillion, or 0.2 picograms of CH_3I in the 5 cm^3 nitrogen sample, is estimated from these chromatograms. For both cases, noise levels can undoubtedly be lowered with more sophisticated electrometer circuitry. With simple low-pass filters, the δI_N and $\delta I_{L/C}$ signal-to-noise responses shown in Figure 14 were improved by about a factor of 3, while the δI_M response was not significantly improved, which is not unexpected since the lock-in amplifier already provides significant noise reduction for the PDM-ECD response. It is also noteworthy that the δI_M response in Figure 14 could be further improved with a more powerful light source. In summary, it appears that the detection limits achievable by the PD-modulated mode of the ECD for a favorable system, such as that demonstrated here for I^-, can be made comparable to those achieved by the normal ECD, and, therefore, can be made competitive with the most sensitive methods available for trace organic analysis.

Sensitivity of the PDM-ECD to CH_3I in the Presence of Excess CCl_4

As part of the sensitivity determination of the PDM-ECD to iodide, an experiment was devised to measure PD of

I^- in the presence of an excess of Cl^-. In order to do this, an exponential diluter was added to the carrier gas line, and enough CCl_4 was injected into the diluter that initially the ECD signal was fully saturated, ie., the standing current went to zero due to the formation of Cl^- by EC by CCl_4. As the CCl_4 concentration in the diluter, and hence the Cl^- concentration in the ECD, was decreased at an exponential rate, the standing current increased accordingly. After enough time had elapsed that the standing current became measurable, injections of 600 pptr CH_3I were made at 6-9 minute intervals and the resulting responses measured.

The results of the experiment are shown in Figure 15, where the relative PD response is plotted against the standing current. Also shown is the normal relative PD response for the same injection with no CCl_4 present. From the results shown in Figure 15, two things are evident. First, the reduction in the standing current due to the presence of CCl_4 does significantly reduce the measured PD response. Secondly, although the responses are reduced, the PDM-ECD is sensitive enough to I^- that CH_3I can easily be detected at low concentration with a standing current as low as about 1 nA, reflecting a background concentration of CCl_4 at least two orders of magnitude greater than that of CH_3I.

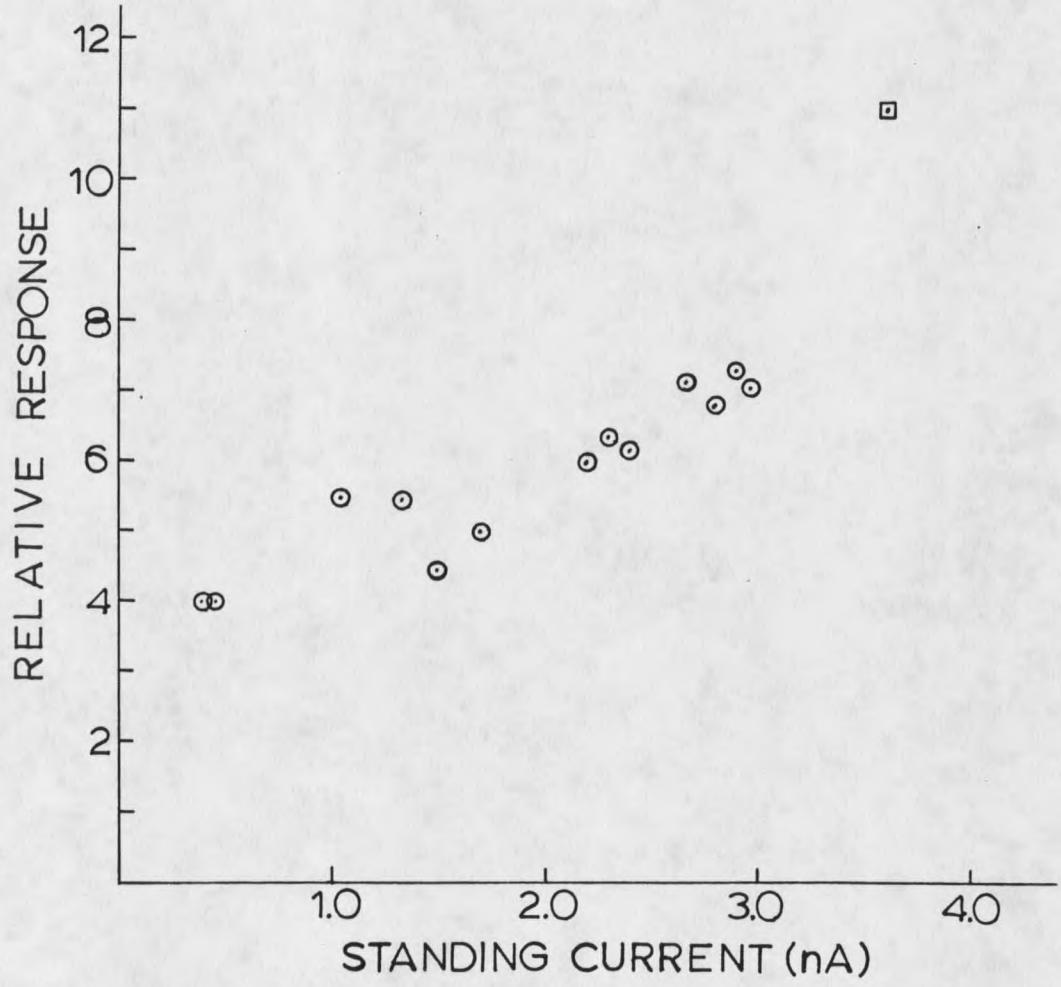

Figure 15. The relative PDM-ECD response ($\delta I_M/\delta I_{L/C}$) to repeated 5 cm^3 gas injections of 600 pptr CH_3I (circles) in a background matrix of CCl_4 which was added into the carrier gas through an exponential dilution volume. The excess CCl_4 caused the standing current to decrease. At a standing current of 1 nA, CCl_4 is still in excess of CH_3I by at least two orders of magnitude. The normal PDM-ECD response to the CH_3I sample without CCl_4 present is also shown (square).

PDM-ECD Study of Nitroaromatic Anions

PD Spectra of the Anions

As was discussed in the Introduction, PD from polyatomic anions has been a useful means of studying thermochemical and spectroscopic properties of negative ions and their photoproducts. In particular, gas phase electron affinities and information on the excited states of negative ions have been obtainable through PD studies.

In this section, the PD spectra of 31 nitroaromatic hydrocarbons will be shown and discussed. These spectra were all obtained at 200°C by the PDM-ECD method under the conditions described in Experimental.

In order to verify the identity of the negative ions formed by EC in the ECD, the APIMS of the compounds were obtained as described in Experimental. With only two exceptions, EC produced a prominent M^- molecular ion and no other fragment ions of intensity greater than 0.1 relative abundance. For o-bromonitrobenzene, the Br^- ion was approximately ten times greater in intensity than the molecular ion. This will also be apparent in its PD spectrum to be discussed later. For m-bromonitrobenzene, the Br^- ion was 0.3 times as intense as the molecular ion. The APIMS measurements also showed the tendency of

p-chloronitrobenzene and p-bromonitrobenzene to form ions of the type $(M + O - Cl)^-$ and $(M + O - Br)^-$, respectively, if oxygen in the carrier gas was not reduced to the lowest possible concentration (53). This phenoxy-type ion formation under ECD conditions will be discussed in more detail in a later section.

Nitrobenzene is representative of the compounds used in this phase of the study. An analysis of a sample containing 400 picograms of nitrobenzene repeated several times at different wavelengths is shown in Figure 16. The magnitude of the δI_N response is about 1.0 nA for each case (total standing current is 4.0nA). In the first case in Figure 16, 525 nm light creates a strong δI_M response, reflecting a large PD cross-section at this wavelength. While in the remaining six analyses the PDM-ECD responses are not large, they are important since they reveal the first detectable onset of PD, λ_{th}, and may bear information on the electron affinity (EA) of the molecule. The λ_{th} determination is difficult because the onset of PD in the threshold region is very weak and gradual. Nevertheless, the absence of a PD response in Figure 16 with 1075 nm and longer wavelengths relative to the responses observed with 1050 nm and shorter wavelengths is distinctly observable above the baseline noise. For nitrobenzene and 30 other nitroaromatics, measurements like these were taken over the wavelength

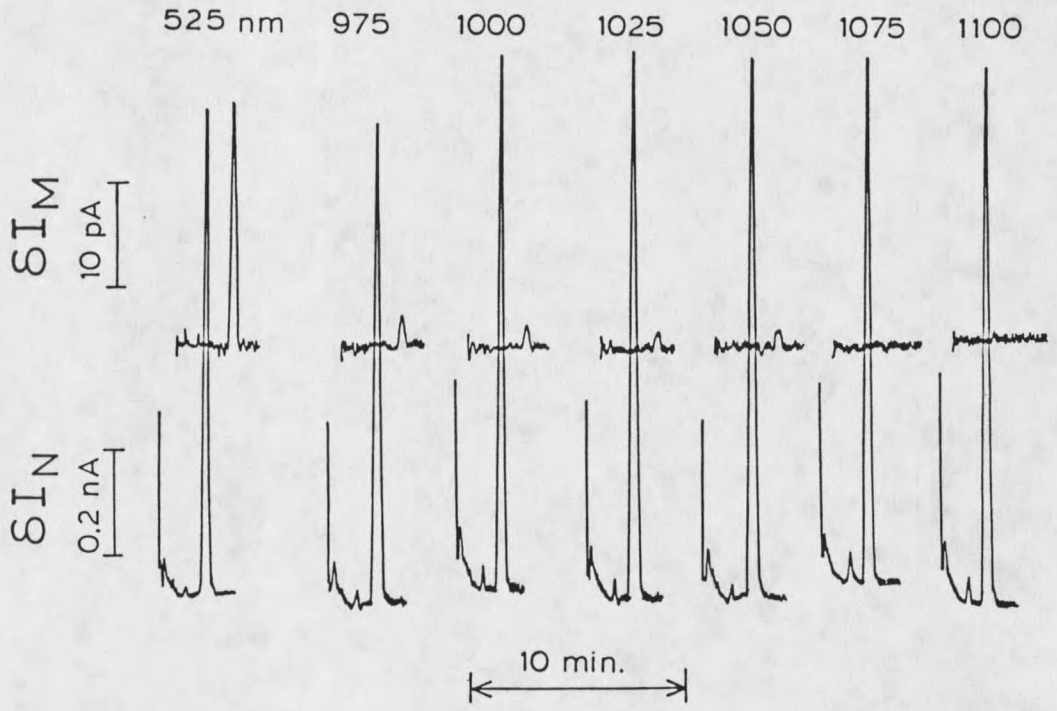

Figure 16. Repeated gas chromatographic analyses by the PDM-ECD of a sample containing 400 picograms of nitrobenzene using the various monochromator settings shown. The two responses simultaneously obtained are the normal ECD response, $\delta I_{L/C}$, and the PDM response, δI_M. The series of long-wavelength analyses shown illustrate the determination of the first detectable PD onset which occurs at λ_{th} = 1050 nm for the nitrobenzene anion.

range of 300-1200 nm at 25 nm intervals.

The spectrum of nitrobenzene is again representative of the other nitroaromatics used in this study, and is shown in Figure 17. The spectrum bears two general characteristics which have previously been reported in other PD studies (54, 55). These two characteristics are: 1) a gradual and continuous increase in the PD cross-section with increasingly shorter wavelengths and (2) the superimposition on this curve of peaks and maxima. The PD mechanisms which have previously been associated with these two characteristics are Direct Photodetachment and Resonance Photodetachment, respectively. A symbolic representation is shown in Figure 18 and will provide the basis for much of the discussions to follow.

The PD spectra for the other nitroaromatics studied are shown in Figures 19-21 and will be addressed at appropriate points in the discussion. For all spectra, the cross-sections measured in the wavelength region of initial PD onset out to 1200 nm are also indicated with x10 amplification by the circled data points. The threshold wavelength, λ_{th}, at which PD is first observed for each case is also indicated in Table 2 along with the energy, E_{th}, of individual photons of that wavelength. The uncertainty in λ_{th} is estimated to be $\pm$ 20 nm and is determined primarily by the monochromator bandpass.

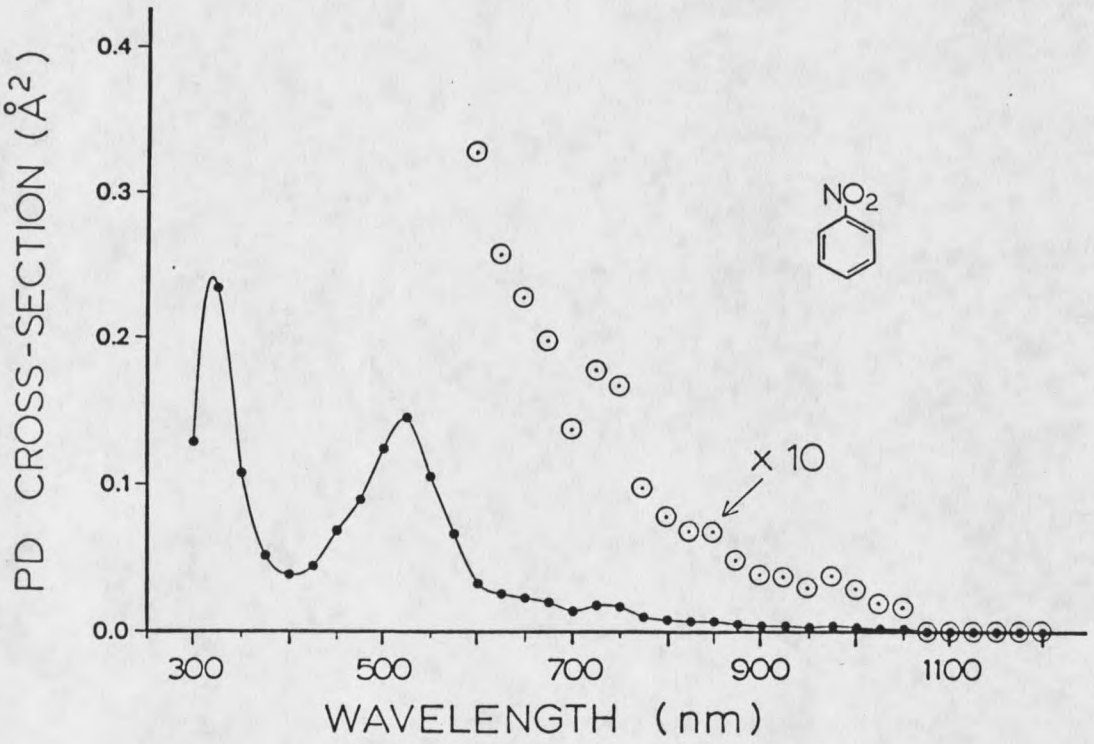

Figure 17. Electron photodetachment spectrum of the molecular anion of nitrobenzene measured by the PDM-ECD at 200°C. Absolute PD cross-sections have been determined by comparisons with the PD measurements of I^- at 365 nm. Measurements have been taken at 25 nm intervals between 300 and 1200 nm. The effective bandwidth of the monochromator is 20 nm for the wavelength settings below 600 nm and 40 nm for settings above 600 nm. The solid line shown is a computer-generated smooth curve passing through the data points.

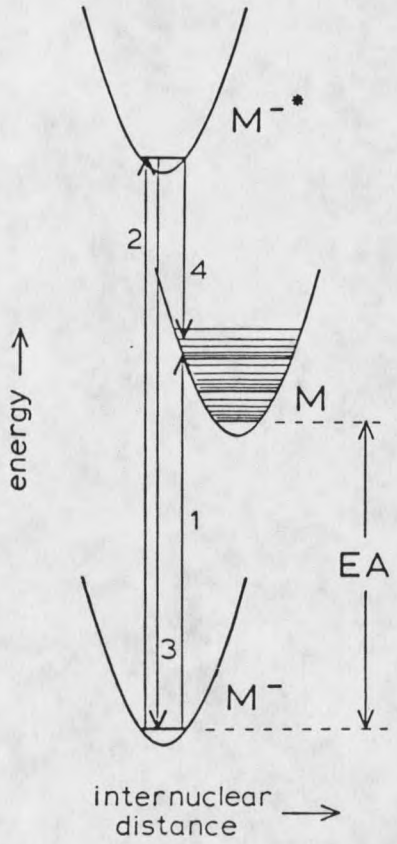

Figure 18. A simple model for the electron photodetachment of nitroaromatic anions. Direct PD is represented by process 1 in which absorption of a photon by M^- leads directly to the neutral molecule and a free electron. Resonance PD is represented by the combination of processes 2 and 4 in which absorption of a photon promotes M^- to an excited electronic state of the negative ion followed either by autodetachment of M^{-*}, process 4, or by relaxation of M^{-*}, process 3. The EA of M is the energy difference between the M and M^- species in their ground electronic, vibrational, and rotational states. The stable structure of the negative ion is shown to be slightly different and somewhat more constrained than that of the neutral molecule.

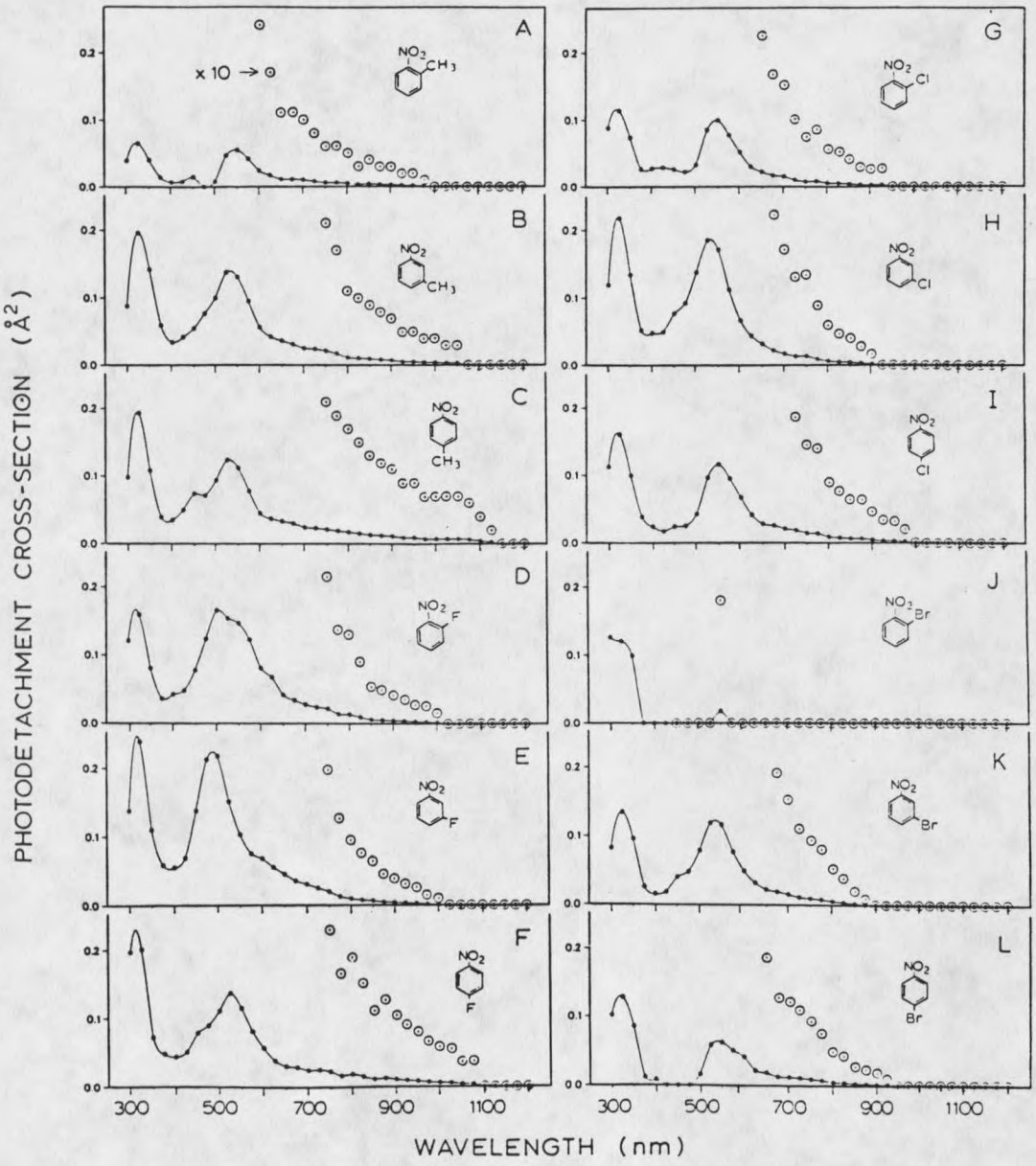

Figure 19. Electron photodetachment spectra observed for twelve substituted nitrobenzenes and dinitrobenzenes by the PDM-ECD at 200°C.

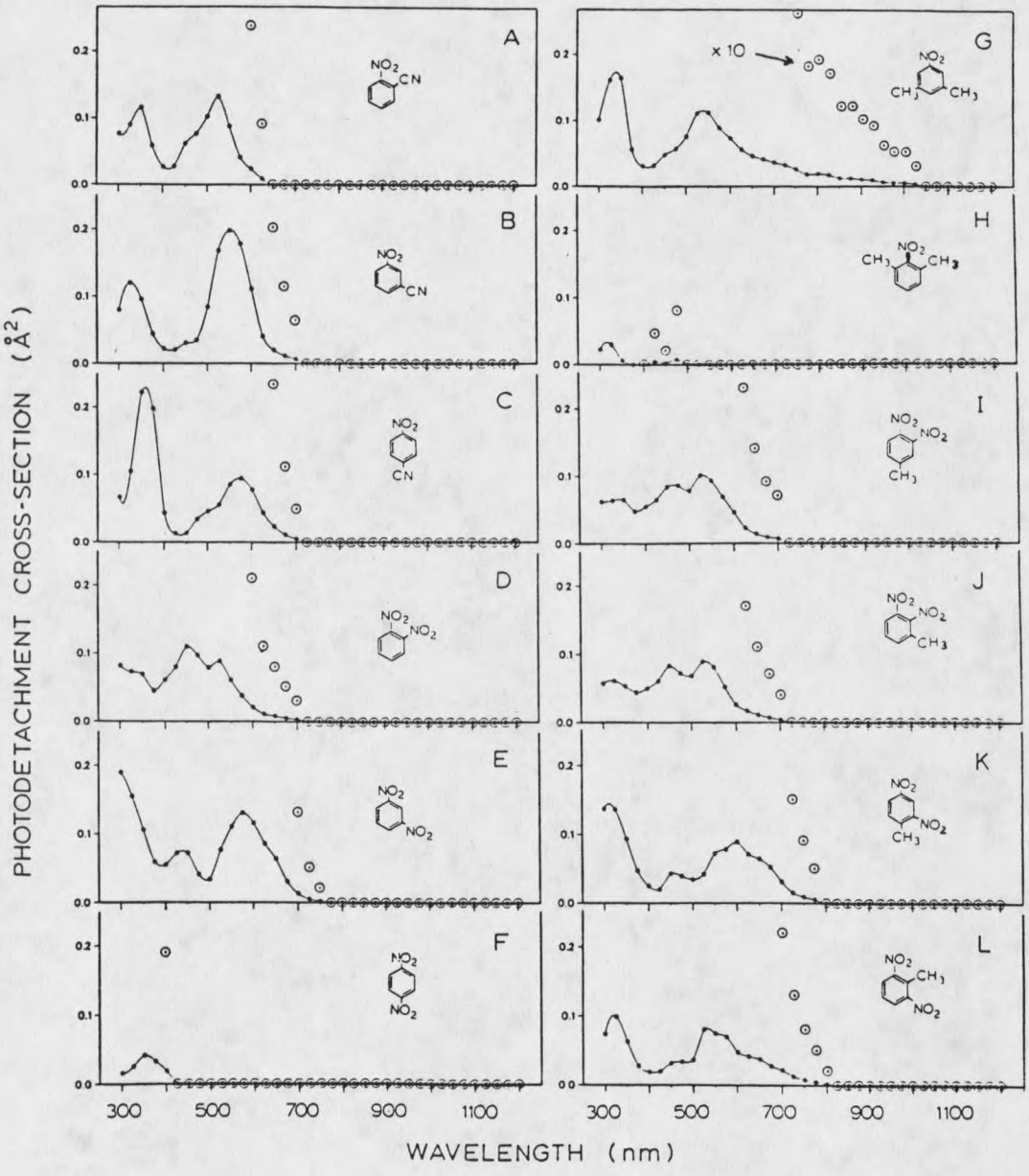

Figure 20. Electron photodetachment spectra observed for twelve substituted nitrobenzenes and dinitrobenzenes by the PDM-ECD at 200°C.

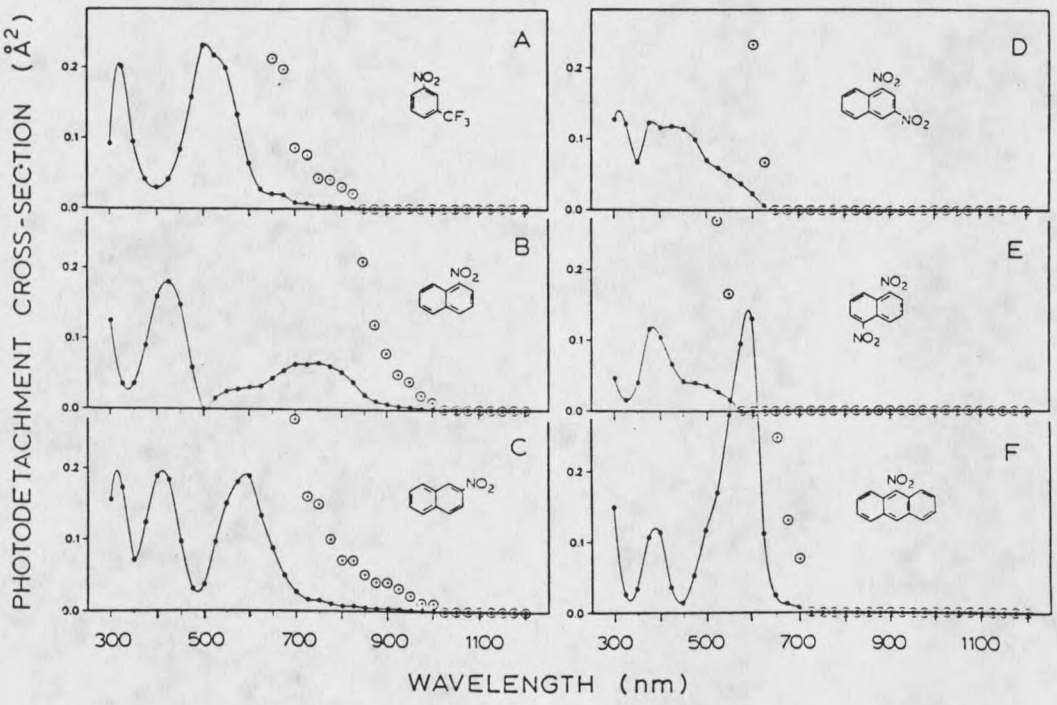

Figure 21. Electron photodetachment spectra observed for six substituted nitroaromatic and dinitroaromatic hydrocarbons by the PDM-ECD at 200°C.

Table 2. Photodetachment thresholds of nitroaromatic anions.

Anion[a]	PDM-ECD[b]		PHPMS[e]	
	λ_{th}(nm)[c]	E_{th}(eV)[d]	EA(eV)[f]	ΔS°(eu)[g]
17) NB	1050	1.18	1.01	-1.0
19A) o-MNB	1000	1.24	0.92	-1.6
19B) m-MNB	1050	1.18	0.99	
19C) p-MNB	1125	1.10	0.95	
19D) o-FNB	1000	1.24	1.07	
19E) m-FNB	1000	1.24	1.23	-1.7
19F) p-FNB	1075	1.15	1.12	
19G) o-ClNB	925	1.34	1.14	-1.6
19H) m-ClNB	900	1.38	1.28	
19I) p-ClNB	975	1.27	1.26	-2.0
19K) m-BrNB	875	1.42	1.32	
19L) p-BrNB	925	1.34	1.29	
20A) o-CNNB	625	1.98	1.61	
20B) m-CNNB	700	1.77	1.56	
20C) p-CNNB	700	1.77	1.72	-2.7
20D) o-DNB	700	1.77	1.65	
20E) m-DNB	750	1.65	1.65	
20F) p-DNB	400	3.10	2.00	-4.5
20G) 3,5-DMNB	1025	1.21		
20H) 2,6-DMNB	475	2.61		

Table 2. (continued)

Anion[a]	PDM-ECD[b]		PHPMS[e]	
	λ_{th} (nm)[c]	E_{th} (eV)[d]	EA (eV)[f]	ΔS° (eu)[g]
20I) 3,4-DNTL	700	1.77		
20J) 2,3-DNTL	700	1.77		
20K) 2,4-DNTL	775	1.60		
20L) 2,6-DNTL	800	1.55		
21A) m-TFMNB	825	1.50	1.41	-2.5
21B) 1-NNAP	1000	1.24	1.23	-0.9
21C) 2-NNAP	1000	1.24	1.18	
21D) 1,3-DNNAP	625	1.98	1.78	
21E) 1,5-DNNAP	550	2.25	1.77	
21F) 9-NANTH	700	1.77	1.43	-2.9

Abbreviations: NB-nitrobenzene; M-methyl; F-fluoro; Cl-chloro; Br-bromo; CN-cyano; D-di; N-nitro; TL-toluene; TF-trifluoro; NAP- naphthalene; ANTH-anthracene.

a The number listed with each anion indicates the figure from which the data was obtained.

b Present work, from Figures 17, 19-21.

c Highest wavelength setting of monochromator at which PD is observed. Uncertainty is ± 20 nm.

d Photon energy corresponding to λ_{th}. Uncertainty is ± 0.05 eV.

e Pulsed high pressure mass spectrometry measurements from reference 57.

f Electron affinity. Uncertainty is ± 0.1 eV.

g Entropy change associated with negative ionization of molecule, $M \longrightarrow M^-$.

Direct Photodetachment and Electron Affinities

Process 1 in Figure 18 represents the direct photon-induced transition of the negative ion, M^-, to produce the neutral product, M, and a free electron. This process is generally expected to be operative in the threshold region of the PD spectrum with photons of energy near that of the adiabatic electron affinity (EA) of M. With photons of progressively higher energy, the PD cross-section is expected to increase in a manner described by the "threshold law" for that system. In order to determine most accurately the EA of a neutral from PD data, ideally the exact threshold law, $\sigma_d(E) = f(E-EA)$, where E is the photon energy, for that system should be known. This knowledge is especially useful if the increase in σ_d with increasing E is very gradual in the region of initial PD onset. Brauman and collaborators (8) have developed considerable understanding of the shapes of PD threshold curves for polyatomic negative ions. They have found that the threshold law for several systems is determined primarily by the symmetry of the highest occupied molecular orbital of the negative ion. They have also shown that additional factors, such as the existence of a strong dipole moment in the neutral, absorption resonances related to excited states of the negative ion and the neutral, and structural differences between the negative

ion and the neutral can also strongly influence the shape and intensity of PD spectra in the threshold region. For the nitroaromatic hydrocarbons studied here, it is suspected that at least some of these complicating factors are operative and would affect any threshold laws which might be derived. Since calculations addressing these factors have not yet been done for the nitroaromatic hydrocarbons, threshold laws cannot be effectively used here. Therefore, only the first detectable onset of PD, λ_{th}, will be used for comparison with the EA of each molecule, while it is recognized that the energy, E_{th}, associated with this wavelength is not necessarily expected to be equal to EA of the molecule.

The M^- ion shown in Figure 18 has been assumed to be in its electronic and vibrational ground state while the photoproduct, M, may be formed in any of a number of vibrational and rotational excited states of its electronic ground state. If the most stable geometries of M^- and M are exactly the same, the first onset of photodetachment of M^- would be observed with photons of energy equal to the EA of M. However, if the stable geometries of M^- and M are significantly different (poor Franck-Condon overlap), as suggested in the case illustrated in Figure 18, the energy, E_{th}, of the photons at the PD threshold will be greater than EA. For the case symbolized in Figure 18, the stable configuration of

M^- is characterized by internuclear distances which are shorter, and intramolecular motions which are more constrained, than those of the parent molecule. This representation has been chosen because Kebarle and coworkers (56, 57) have shown that the entropy of negative ionization, ΔS° for the process $M \longrightarrow M^-$, is consistently negative for nitrobenzene and for substituted nitroaromatic hydrocarbons, in general. They suggest that this loss of entropy upon addition of an electron to these molecules is due to a stiffening of the internal rotation of the NO_2 groups due to increased π character in the C-N bond of the anion.

For all of the nitroaromatic hydrocarbons studied here, with the exception of o-bromonitrobenzene noted previously, the first onset of PD indicated in Figures 19-21 is thought to be due to the photodetachment of the M^- species. These threshold measurements, λ_{th} and E_{th}, are listed in Table 2, along with values for the adiabatic EA and the entropy of negative ionization for many of the nitroaromatic hydrocarbons. These thermochemical properties have recently been determined by Kebarle and coworkers (56-58) through observations of gas phase electron transfer equilibria by pulsed high pressure mass spectrometry (PHPMS). A comparison of the E_{th} values observed here with Kebarle's EA determinations is also provided graphically in Figure 22. The dashed

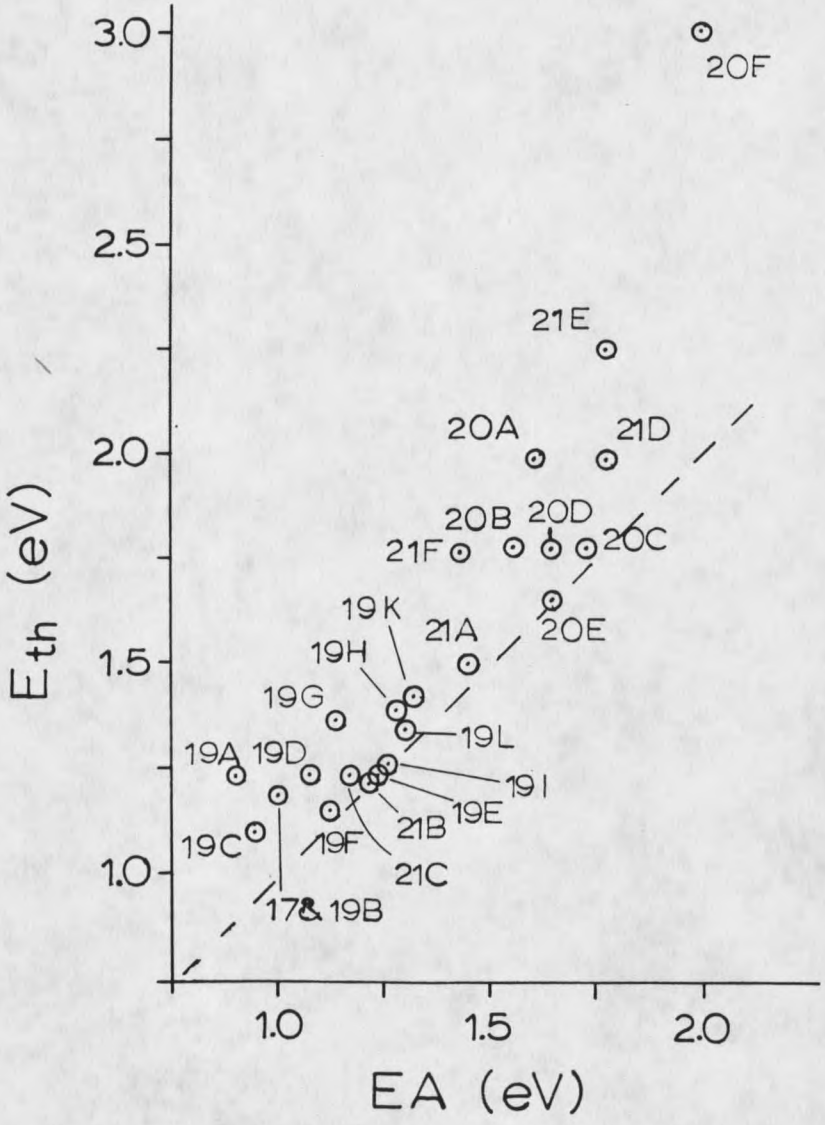

Figure 22. PD threshold energies, measured by the PDM-ECD, plotted against the adiabatic electron affinity (EA) of the corresponding nitroaromatic molecules determined from the electron transfer reactions by Kebarle and coworkers (56-58). The numbers shown indicate the compound and PD spectra in Figures 19-21 associated with each data point. The dashed line is the line on which all points would lie if E_{th} = EA for each case.

line shown in Figure 22 has unity slope and is the line on which all points would fall if E_{th} = EA.

Given the estimated uncertainty indicated with each set of energy measurements, many of the comparisons made in Figure 22 do lie sufficiently close to the dashed line as to indicate that the measurements of E_{th} for these are essentially equal to the corresponding adiabatic EA values of Kebarle and coworkers (56-58). Nevertheless, approximately one-half of the data set clearly indicates that E_{th} exceeds EA by an amount greater than the uncertainty of the two measurements. In view of expected geometry differences between the M^- and M species of the nitroaromatic hydrocarbons (56, 57), the result that E_{th} exceeds EA is not unexpected. The only result which would not have been consistent with the simple model shown in Figure 18 would have been if E_{th} had been found to be less than EA for any of the compounds studied. This result would be expected only if the M^- ion possessed sufficient internal energy so that its higher vibrational states were well-populated and photons having less energy than the adiabatic EA could cause direct PD. As has been previously explained, however, only ions of relatively low internal energy will be present in an atmospheric pressure ion source.

Correlations might be expected to exist between the magnitude of the difference between the E_{th} and EA values

discussed above and Kebarle and coworkers (56, 57) ΔS° values for negative ionization, since both of these are thought to be related to the magnitude of structural differences in the M^- and M species. Unfortunately, the estimated uncertainty of the ΔS° values and the differences in E_{th} and EA values are too large to allow a meaningful comparison of this type to be made for many of the cases indicated in Table 2 and Figure 22. Nevertheless, for a few cases in which the differences between E_{th} and EA are unusually large, comparisons with the corresponding ΔS° values do suggest the existence of a direct correlation. For example, the greatest departure from the dashed line in Figure 22 is data point 20F for p-dinitrobenzene. In strong contrast, data points 20D and 20E for the ortho- and meta- isomers of dinitrobenzene lie very close to the unity slope dashed line. As indicated in Table 2, Kebarle and coworkers (56, 57) found p-dinitrobenzene to possess the most negative ΔS° value, -4.5 cal/°K, of the group of compounds they studied (unfortunately, the ortho and meta isomers of dinitrobenzene were not included in that study). Therefore, both the PDM-ECD and the PHPMS experiments indicate that an unusually great geometry change accompanies the addition of an electron to p-dinitrobenzene.

The significant structural change which occurs in the negative ionization of p-dinitrobenzene may be due to the relative importance of resonance form I in Figure 23 in determining the structure of the molecular anion, while the analogous resonance form of the neutral molecule would not be expected to be as important in influencing its structure.

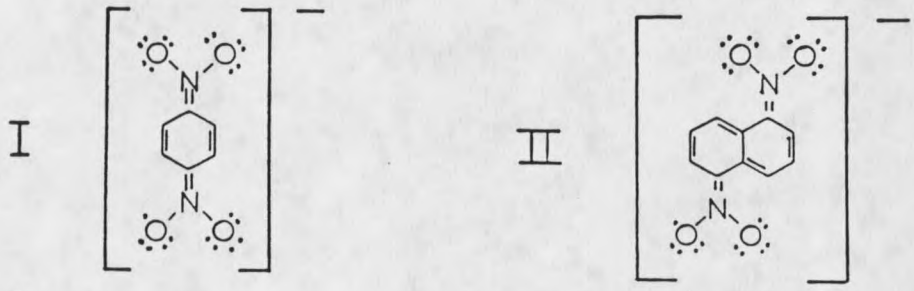

Figure 23. Possible resonance forms for (I) p-dinitrobenzene and (II) 1,5-dinitronaphthalene showing a stiffening of the C-N bonds and hindered rotation of the NO_2 groups due to the double bond character of the C-N bonds.

In resonance form I, considerable stiffening of both C-N bonds and the hindered rotation of both NO_2 groups is expected due to the double-bond character assumed by both C-N bonds. Other reasonable resonance forms can be written for this anion in which one or both of the C-N bonds have sigma character, however, none of these would include a larger number of conjugated double bonds than the four shown in resonance form I and, therefore, would not necessarily be favored over form I. By removal of

one electron from form I, a potential resonance structure for neutral p-dinitrobenzene can be written which also has four conjugated double bonds. However, for the neutral, competing resonance structures having C-N bonds of sigma character can be written in which five conjugated double bonds are present. Therefore, the greater resonance energy of these competing forms will diminish the contribution of form I to the structure of neutral p-dinitrobenzene.

The resonance form argument is also consistent with the results for other dinitroaromatic hydrocarbons studied here. A resonance form of type I, in which both C-N bonds assume π character, is not possible for m-dinitrobenzene and no anomalously large structure change was suggested by its E_{th} measurement. For o-dinitrobenzene, a resonance form analogous to type I would not be favored due to steric hindrance and, again, E_{th} for this compound was not found to be significantly larger that its EA.

The case of 1,5-dinitronaphthalene indicated by data point 21E in Figure 22 deviates significantly from the unity slope dashed line, suggesting that a significant structure change accompanies its negative ionization. For the 1,5-dinitronaphthalene anion, resonance form II in Figure 23 is possible in which the π-resonance system is extended over the entire molecule by six conjugated

double bonds, two of which are the C-N bonds. Competing resonance forms having a greater number of double bonds cannot be written for this anion. On the other hand, the resonance form of type II for the neutral molecule will have one fewer double bond than its competing resonance structures and is not expected to be as important in determining the structure of the neutral. A resonance form of type II is not possible for the 1,3-dinitronaphthalene anion and, as shown by data point 21D in Figure 22, the departure of its E_{th} value from the unity slope dashed line is much less severe than that of the 1,5- isomer, even though the EA values of these two isomers are identical.

Another systematic trend, consistently noted in Table 2 and in Figure 22, is that the difference between E_{th} and EA for all of the methyl-, fluoro-, chloro-, and cyano-substituted nitrobenzenes is always greatest for the ortho isomer. This suggests that the magnitude of geometry change upon the negative ionization of these molecules is greatest for the ortho isomers. Unfortunately, this trend in the PD spectra can not presently be compared with parallel ΔS° determinations from PHPMS because too few of these have been made to date.

Resonance Photodetachment

The peaks and maxima observed in the PD spectra of the nitroaromatic anions in Figures 19-21 cannot be attributed to an alternate form of the Direct PD mechanism in which a transition from M^- to an electronically excited state of M might be envisioned. Resonances and peak maxima are not expected to be associated with transitions of this type (11, 12). Furthermore, electronic excited states of sufficiently low energy are not thought to exist for most of the neutral nitroaromatic hydrocarbons studied here. For example, the peak at 525 nm in the PD spectrum of nitrobenzene anion shown in Figure 17 cannot be attributed to Direct PD of M^- to form an excited electronic state of M. The UV-Vis absorption spectrum of molecular nitrobenzene contains no absorption in the wavelength range greater than 400 nm (59) which indicates that no excited states of nitrobenzene exist within 3.0 eV of its ground state.

As shown in Figure 18, the other mechanism by which PD can occur is initiated by process 2, the absorption of light by M^- to form the electronic excited state, M^{-*}. The excited negative ion can then either relax back to its ground state by radiative or non-radiative processes, shown collectively as process 3, or can undergo autodetachment to form the neutral molecule and an

electron, shown as process 4. Since the energies of excited electronic states of negative ions are often greater than the EA of the neutrals, this process is potentially available to most negative ions. The criteria required for this mechanism to lead to intense resonances and peaks are that the cross-sections for absorption, σ_a, must be larger than the cross-sections for Direct PD somewhere in the spectral region above E_{th}, and the quantum efficiency for autodetachment, given by $\Phi = k_4/(k_3 + k_4)$, must be acceptably high.

If the photodetachment peaks in Figures 19-21 are due to Resonance PD, the PD spectrum observed for each compound should resemble the absorption spectrum of the negative ion. Shida and Iwata (60) have provided the absorption spectra of numerous nitroaromatic anions which were made and contained in τ-irradiated glassy solutions frozen at 77°K. Some of their results have been plotted in Figure 24 (continuous curves) in a form (molar absorptivity coefficients have been converted to cross-sections, wavenumbers to wavelengths) which facilitates their comparison with the corresponding PD spectra reported in Figures 19-21. The gas phase PD measurements for each anion are also shown (points) in Figure 24.

The absorption spectrum of nitrobenzene anion, shown in Figure 24A, bears an obvious and convincing resemblance to its PD spectrum. In both spectra, a

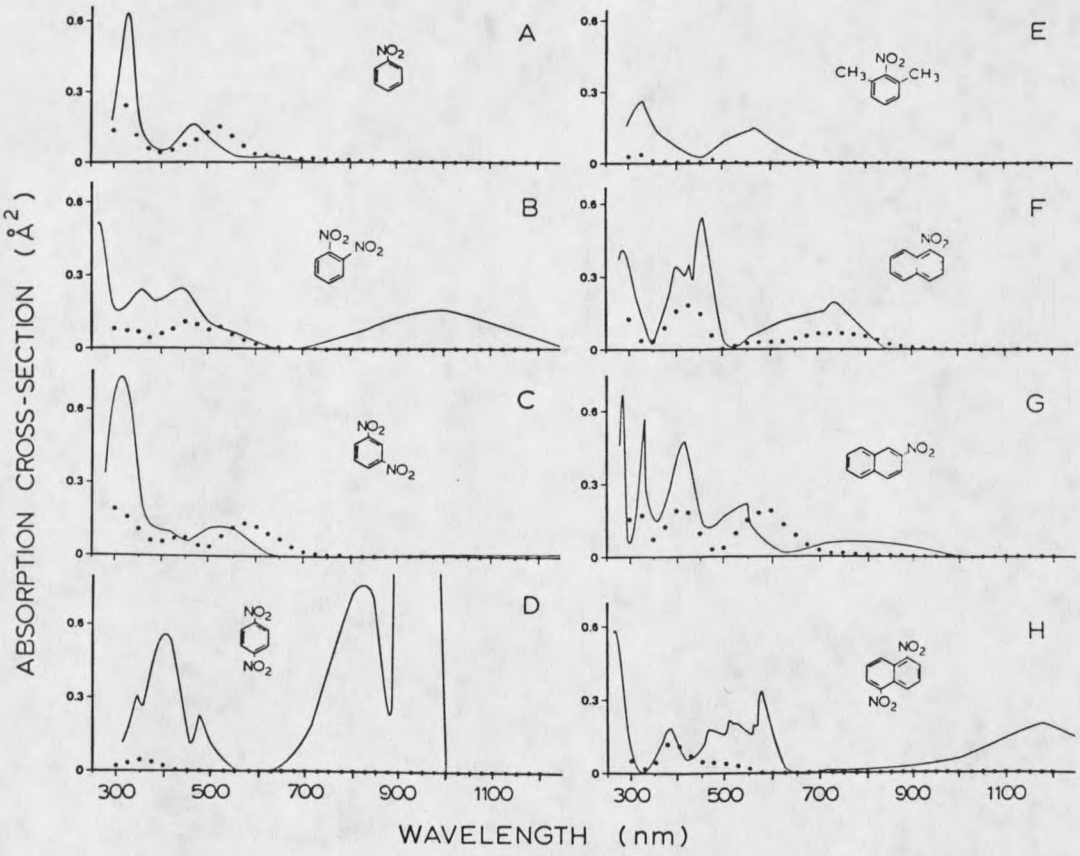

Figure 24. The absorption spectra (continuous curves) of the molecular radical anions of several nitroaromatic hydrocarbons reported previously by Shida and Iwata (60). The molecular anions were formed by τ-irradiation of glassy solutions frozen at 77°K. These data have been converted to a form which facilitates their comparison with the PD spectra of the corresponding molecular anions which are shown in Figures 19-21 and have been replotted here (points).

large peak is noted at 325 nm and another, in the 500 nm region. The latter peak is red-shifted about 50 nm in the PD spectrum relative to that of the absorption spectrum. Red shifts of this magnitude have been observed previously in comparisons of gas phase to condensed phase electronic spectra (55) and have been attributed to solvation effects which can increase the energy of certain electronic transitions by destabilizing an excited state relative to the ground state (61). The σ_a values for absorption at the two peak maxima in Figure 24A are very large (a σ_a value of 0.6 $Å^2$ corresponds to a molar absorptivity of $\epsilon = 1.6 \times 10^4$ cm^{-1} M^{-1}) with one equal to and the other about twice as great as the two corresponding σ_d values. Due to the considerable differences in physical conditions under which the absorption and the PD measurements were made, quantitative deductions as to the relative rates of processes 2-4 in Figure 18 in terms of the observed σ_a and σ_d values for nitrobenzene would not be expected to be very accurate. Nevertheless, these cross-section measurements at the absorbance and PD maxima do clearly indicate that process 2 is very efficient for the gas phase nitrobenzene anion and that the quantum efficiency, Φ, for PD is quite high for both of the excited states of the negative ion indicated in the spectrum. Using the σ_a and σ_d values without correction for phase and

temperature differences indicates $\Phi = \sigma_d/\sigma_a \approx 0.5$ at 325 nm.

Shida and Iwata (60) also measured the absorption spectra of the three isomers of methylnitrobenzene anion and found that they differed very little from that shown for nitrobenzene anion in Figure 24A. In Figures 19A-19C, the PD spectra of the three isomers of methylnitrobenzene are shown and these are quite similar to the PD spectrum of nitrobenzene anion. Contrary to the absorption spectra reported by Shida and Iwata (60), however, the PD cross-section for the ortho isomer in Figure 19A is significantly reduced relative to those of nitrobenzene and the meta and para isomers of methylnitrobenzene anion. The absorption spectrum of 2,6-dimethylnitrobenzene in Figure 24E shows the effect on absorption of having two methyl groups adjacent to the nitro group. Only the higher energy absorption maximum observed at 325 nm is noticeably weakened relative to that of the nitrobenzene anion. While the absorption maximum at 575 nm has been red-shifted about 100 nm, its intensity is undiminished. The PD spectrum of 2,6-dimethylnitrobenzene anion shown in Figure 20H indicates that the σ_d values are greatly reduced at all peak maxima relative to that of nitrobenzene anion. The PD spectrum of 3,5-dimethylnitrobenzene anion, shown in Figure 20G, exhibits peak maxima as intense as that of nitrobenzene

anion. The results indicate that methyl substitution adjacent to the nitro group tends to decrease σ_d much more than it does σ_a at the peak maxima. In terms of the model for PD illustrated in Figure 18, this result suggests that methyl substitution in the ortho position has relatively little effect on process 2, but substantially decreases the quantum efficiency for Resonance PD by decreasing the rate of autodetachment, process 4, relative to that of relaxation, process 3. In the previous section dealing with Direct PD, it was noted that any substitution, including methyl, at the ortho position of nitrobenzene was shown to cause E_{th} to significantly exceed EA and this was suggested to be caused by poor Franck-Condon overlap of the M^- and M species. Poor Franck-Condon overlap of the M^{-*} and M species would also be expected if the M^- and M^{-*} states of the anions have very similar structures as implied in Figure 18. Therefore, it is reasonable to suggest that the lower σ_d values observed here with methyl substitution at the ortho position are also caused by poor Franck-Condon factors and, for the Resonance PD mechanism, this causes the rate of process 4 and the magnitude of Φ to be decreased. That the M^- and M^{-*} species of o-methylnitrobenzene anion do, in fact, have similar structures is supported by the fact that σ_a of its two absorption maxima (60) are large.

The matrix absorption spectra of the ortho and meta isomers of dinitrobenzene anion, shown in Figures 24B and 24C, also bear considerable resemblance to the gas phase PD spectra of these anions. The ortho isomer, for example, has a unique multiplicity of peaks in the short wavelength region which is evident also in its PD spectrum shown in Figure 20D. For this anion, the broad absorption which reaches a maximum at 1000 nm in Figure 24B is not expected to be seen in the corresponding PD spectrum because the excited electronic state of the negative ion involved in this transition lies below the EA of this molecule and, therefore, it is not capable of autodetachment. These low-energy excited electronic states are present in other molecules as well. For example, the intense absorption peaks shown in Figure 24D for p-dinitrobenzene anion at wavelengths longer than 700 nm are not expected to be seen in the PD spectrum since the very high EA of p-dinitrobenzene (2.0 eV) prohibits Resonance PD with wavelengths greater than about 600 nm.

In Figure 24D, the absorption spectrum of p-dinitrobenzene, it should also be noted that σ_d for the peak maximum at 350 nm is greatly reduced relative to σ_a for the absorption peak of this anion at 400 nm. This result is consistent with the effects of ortho-methyl substitution, discussed previously, in which a decrease in σ_d at peak maxima was attributed to poor Franck-Condon

factors. In the section concerning Direct PD, particularly poor Franck-Condon factors were indicated for p-dinitrobenzene.

The PD spectra of several methyl-substituted dinitrobenzenes are also shown in Figure 20. A comparison of Figures 20D, 20I, and 20J indicate that little change in the PD spectrum of o-dinitrobenzene is caused by the addition of a methyl group to either of the two possible positions on its ring. On the other hand, a comparison of PD spectra 20E, 20K, and 20L indicate a progressive decrease in σ_d of the m-dinitrobenzene isomer at the peak maxima as the methyl group is placed first adjacent to one and then adjacent to both of the nitro groups. This result for methyl-substituted m-dinitrobenzene is consistent with the effects of o-methyl substitution on the σ_d of nitrobenzene anion, discussed above. The fact that a much smaller effect on σ_d is caused by methyl substitution in o-dinitrobenzene anion is undoubtedly due to the large degree of steric hindrance already caused by adjacent NO_2 groups. Therefore, the additional steric effect caused by an added methyl group is not as important.

The absorption spectra of 1- and 2-nitronaphthalene anions shown in Figures 24F and 27G provide a particularly interesting comparison with their PD spectra. The absorption spectrum of each of these is

unique and relatively complex. Nevertheless, their essential features are apparent in the PD spectra of these two anions shown most clearly in Figures 21B and 21C.

Phenoxy-type Ion Formation in the PDM-ECD

As discussed earlier, APIMS measurements have shown the tendency of certain molecules such as o- and p-chloronitrobenzene and p-bromonitrobenzene to form phenoxy-type ions, $(M + O - Cl)^-$ or $(M + O - Br)^-$, under ECD conditions if great care is not taken to minimize oxygen levels in the ECD. Oxygen can contaminate the ion source through leaks in gas transfer lines or the ECD itself, or as an impurity in the carrier gas. For the PDM-ECD experiments, leaks were minimized by maintaining a positive pressure within the ECD with a flow restrictor on the gas outlet port. However, if trace oxygen levels in the carrier gas were large enough to form the phenoxy-type molecules, there would be some uncertainty as to the identity of some of the ions produced in the ECD. In order to determine if this was occurring, oxygen was intentionally introduced into the carrier gas with an exponential dilution volume. By adding a small quantity of pure oxygen to the diluter, an oxygen concentration of at least 10 ppm was continually supplied to the ECD during the course of the experiment. Dzidic, Caroll, Stillwell,

and Horning (53) have determined that for phenoxy ion formation, $k = 3 \times 10^{-11}$ cm^3 $molecules^{-1}$ s^{-1}. For an oxygen concentration of 10 ppm (2.5×10^{14} molecules cm^{-3}), this produces a pseudo-first order rate constant of 7500 s^{-1}, much faster than positive ion-negative ion recombination (100 s^{-1}) or PD (about 10 s^{-1}), the two competing reactions.

An experiment was done to compare the PD spectra of compounds with and without oxygen added to the system. Five compounds were chosen, two of which, o- and p-chloronitrobenzene, are known to form phenoxy ions with oxygen present, and three of which, iodooctane, m-chloronitrobenzene, and p-fluoronitrobenzene, will not form phenoxy ions. If the spectra of either o- or p-chloronitrobenzene are substantially different under conditions favoring phenoxy ion formation (oxygen added) compared to normal conditions (no oxygen added), this would indicate that under normal conditions, the species present are predominantly molecular ions. If, on the other hand, the spectra of o- and p-chloronitrobenzene remain unchanged, this would indicate that the phenoxy ions are formed in the ECD under both conditions. The spectra of m-chloronitrobenzene and p-fluoronitrobenzene are not expected to change since neither tend to form phenoxy-type molecules under these conditions.

The results are shown in Figure 25 and indicate that the PD cross-section for m-chloronitrobenzene is unaffected or slightly enhanced by the addition of oxygen. This was also observed for p-fluoronitrobenzene (not shown). On the other hand, the PD cross-sections for o- and p-chloronitrobenzene are reduced by about 50 percent from 300-325 nm and 525-600 nm, and are eliminated entirely over the rest of the wavelength range. This large change would seem to indicate that with oxygen added, o- and p-chloronitrobenzene form different ions, presumably phenoxy-type ions, in addition to molecular ions under ECD conditions. The PD responses observed for these compounds at 300-325 nm and 525-600 nm, which correspond to the peaks observed with no oxygen added, probably indicate that some molecular ions are still present, or that the new ions also PD at these wavelengths.

The PD cross-section of I^- was decreased by about 30 percent by the addition of oxygen. It should be noted, however, that the molecular ion cross-sections were determined relative to I^- and should indicate the absolute cross-section. The observed reduction for I^- was probably due to the reduced standing current resulting from the added oxygen. Reduced responses at lower standing currents have been observed under other conditions also, such as impurities being present in the ECD.

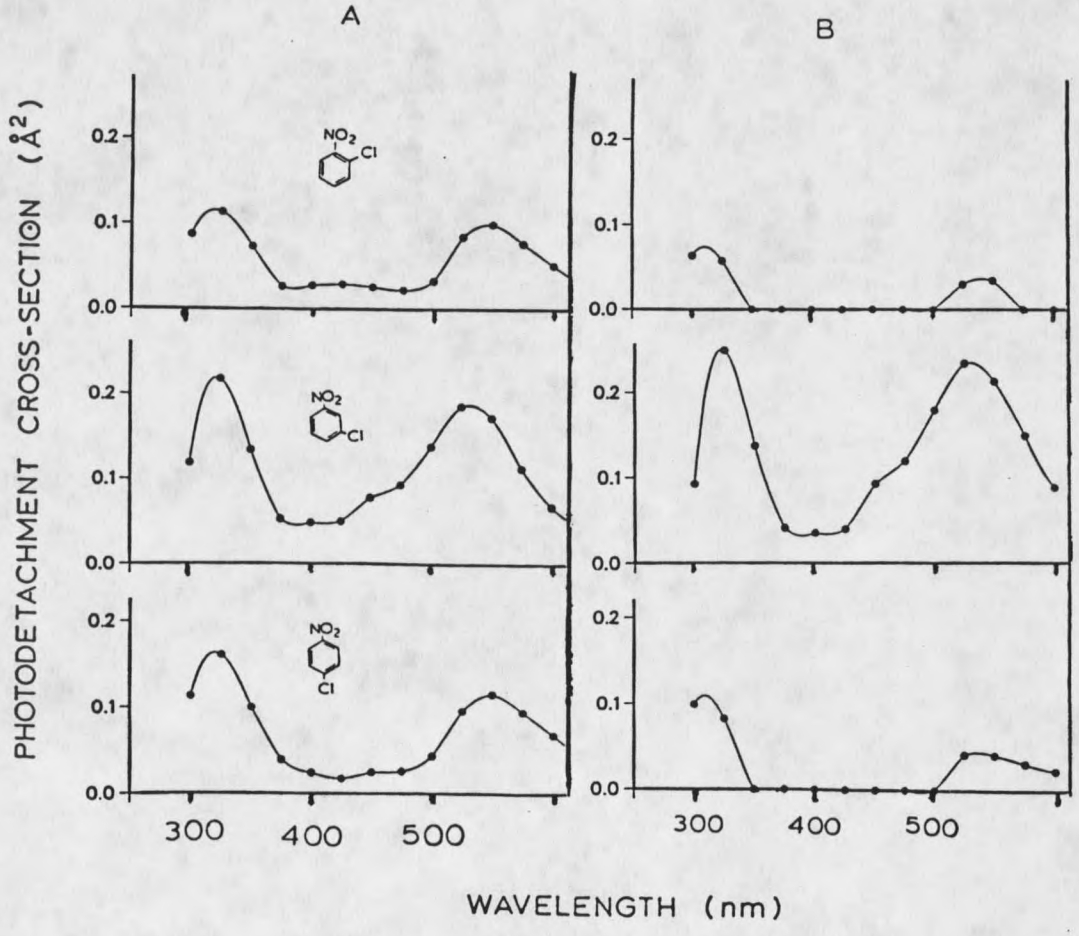

Figure 25. PD spectra of the three isomers of chloronitrobenzene. The spectra in column A were obtained under normal PDM-ECD conditions. The spectra in column B were obtained with approximately 10 ppm oxygen included in the nitrogen carrier gas.

The results seem to indicate that under normal PDM-ECD conditions, oxygen is not present in high enough concentrations to affect substantially the molecular ion population, even of compounds particularly susceptible to phenoxy ion formation.

PDM-ECD Study of Quinone Anions

Quinone and two other members of the quinone family, fluoranil (tetrafluoro-1,4-benzoquinone) and chloranil (tetrachloro-1,4-benzoquinone), were studied with the PDM-ECD. The quinone family has been studied extensively elsewhere due to its importance in some biological systems. The quinone, fluoranil, and chloranil molecules will rapidly attach electrons in the ECD to form radical anions which will undergo PD.

PD Spectra and EA of p-Benzoquinone

The photodetachment spectrum of the p-benzoquinone anion is shown in Figure 26. As with all the molecular ions previously discussed, peaks are observed in the spectrum, which are attributed to resonance PD.

The PD behavior of p-benzoquinone has been studied and reported previously. Holroyd (62) obtained a spectrum by laser PD in several non-polar liquids. A double-pulse conductivity technique was used, where the first pulse was an x-ray pulse which liberated electrons

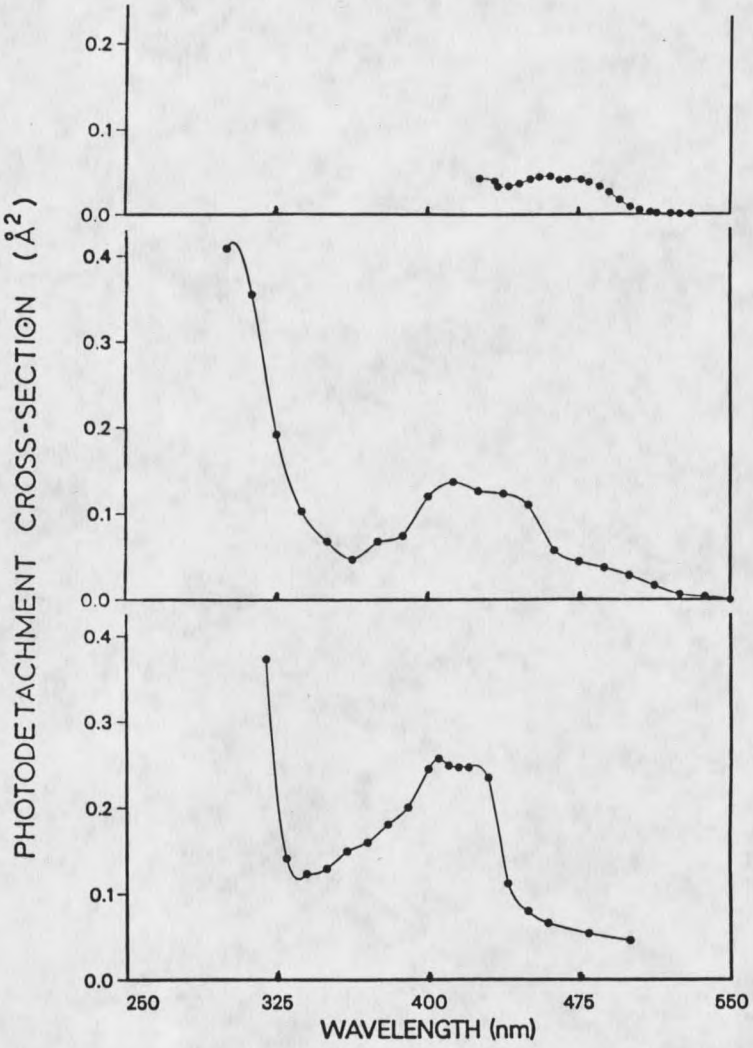

Figure 26. Spectra of p-benzoquinone. The top spectrum is the PD spectrum obtained by Holroyd (62) in liquid trans-stilbene using a pulse radiolysis technique. The middle spectrum is that obtained by the PDM-ECD in nitrogen. The bottom is the UV-Vis absorption spectrum in aqueous phase obtained by Adams and Michael (63).

to react and form benzoquinone anions. The second pulse was from a tunable dye laser after a delay period of 10 to 200 μs. The PD cross-section was obtained from the amplitude of the current signal (due to the electrons detached from the anion) during the laser pulse. The resulting spectrum obtained in trans-stilbene is also included in Figure 26.

A comparison of the two spectra indicates that, in general, the PD cross-section is somewhat smaller in the liquid-phase than in the gas-phase. It is not known if this is to be expected since, to my knowledge, there have been no published reports comparing the magnitudes of PD cross-sections in the two different phases. The same peak shapes or trends seem to be evident in both spectra down to 425 nm, the low wavelength limit for the laser. Unfortunately, the liquid phase spectrum is only over a small wavelength range making it difficult for useful comparisons to be made.

Also shown in Figure 28 is the UV-Vis absorption spectrum of benzoquinone obtained by Adams and Michael (63) in an aqueous solution. The absorption was determined by a pulse-radiolysis experiment similar to that done by Holroyd (62) except that absorption, rather than PD, was measured. The similarities between the absorption and PD spectra are quite evident.

The λ_{th} values can be used to calculate an E_{th} for p-benzoquinone. For the PDM-ECD method, λ_{th} = 537.5 nm, and for the liquid phase experiment, λ_{th} = 535 nm. Considering the resolution used in the PDM-ECD experiment, these are identical results, which lead to E_{th} = 53.4 kcal/mol. Chowdhury, Heinis, Grimsrud, and Kebarle (57), using an electron-transfer equilibrium technique, reported a value of EA = 44.1 kcal/mol. As discussed in the section on the nitroaromatics, this difference is not unexpected, due to possible geometry differences between the anion and the neutral. Kebarle and coworkers (57) do, in fact, report ΔS° = -4.0 eu for p-benzoquinone, which indicates a relatively large geometry difference between the neutral and the anion, with the anion being in a more constrained configuration.

Marks, Comita, and Brauman (64) have also studied the PD behavior of p-benzoquinone. Their technique produces anions in an ion cyclotron resonance mass spectrometer and obtains a PD spectrum by measuring a decrease in the ion signal upon laser irradiation. The particular study cited (64) dealt with dipole-supported states and compared only the PD threshold regions of o- and p-benzoquinone. Although an entire spectrum was not published, they assign a PD threshold value for p-benzoquinone as λ_{th} = 624 nm providing a value of E_{th} = 45.8 kcal/mol, virtually identical with the EA value

determined by Kebarle and coworkers (57). The fact that the ICR method provides a λ_{th} value 100 nm different from the PDM-ECD method may indicate a greater sensitivity for the ICR method. Considering the high ion monitoring sensitivity for ICR's and the high power of lasers, this is not unexpected. The drawback to the ICR method, as discussed in the Introduction, is that it is often difficult to form ground state anions in the low pressure ICR cavity.

PD Spectra and EA of Chloranil and Fluoranil

The other two members of the quinone family studied with the PDM-ECD were fluoranil and chloranil. Their PD spectra are shown in Figure 27. The two spectra are similar except that chloranil shows a peak at approximately 320 nm, whereas the cross-section for fluoranil continues to increase in the short wavelength range of the experiment, and is much larger. Assuming that fluoranil has a peak which corresponds to the 320 nm peak for chloranil, it has apparently been blue-shifted by at least 25 nm, and is much larger. No such shift was observed for the fluoronitrobenzenes compared to the chloronitrobenzenes shown in Figure 19. This shift may be unique to the quinones, or may be due to the presence of four halogens on the molecules.

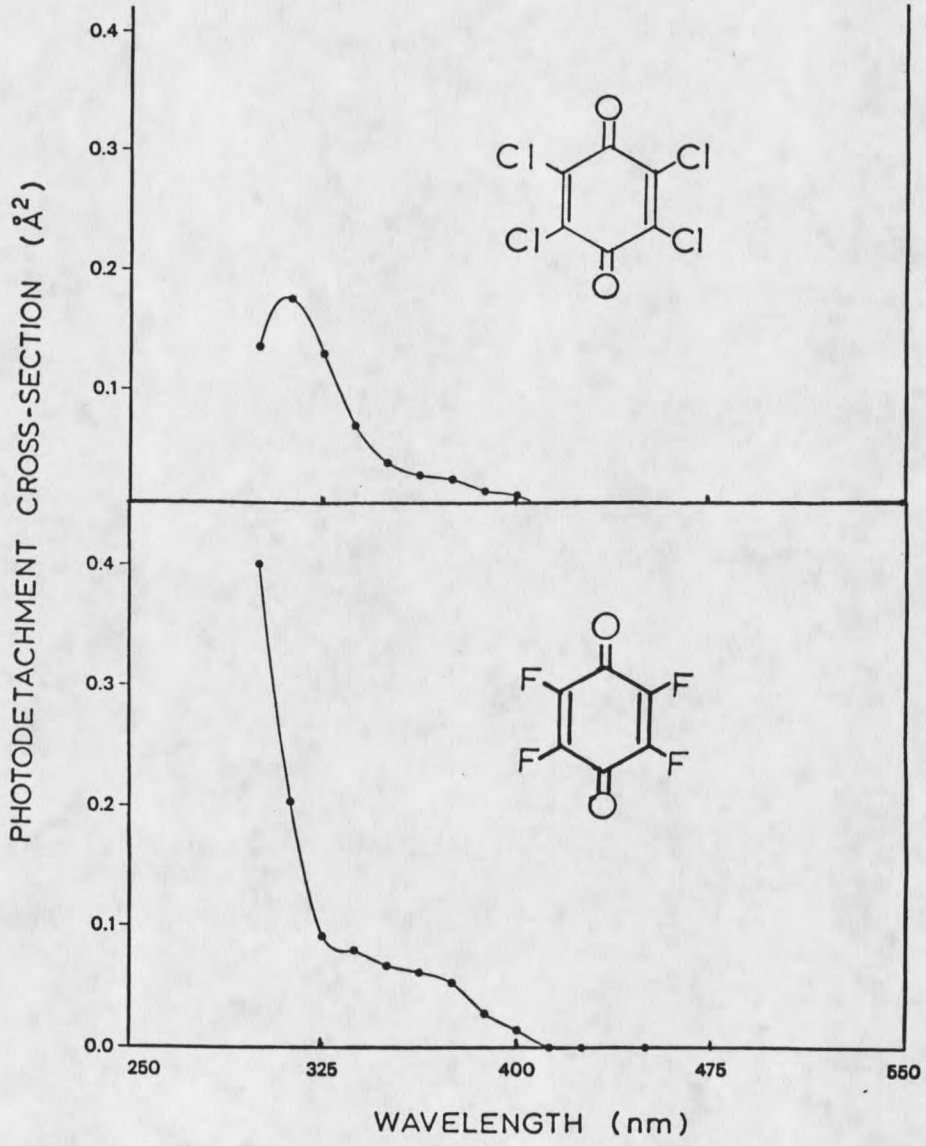

Figure 27. PD spectra of chloranil and fluoranil at 150°C obtained with the PDM-ECD.

For both fluoranil and chloranil, λ_{th} = 400 nm, which corresponds to E_{th} = 71.5 kcal/mol. Kebarle and coworkers (57) report values of EA = 62.3 kcal/mol and 64.0 kcal/mol, respectively. For both compounds, the reported (57) value of $\Delta S°$ = -3.5 eu indicates a relatively large geometry difference between the anions and the neutrals, which could account for the difference between the E_{th} and EA determinations.

PDM-ECD Study of Several Perfluorinated Compounds

Although there have been extensive studies on electron capture, electron transfer, and EA of some perfluorocarbons (57, 58, 65, 66), very little has been reported on PD of these compounds. The fast electron capture rates of these compounds and their relatively low EA values (57, 58, 65, 66) would seem to indicate that they are prime candidates for study in the PDM-ECD.

The electron attachment and detachment for SF_6, in particular, have been studied extensively (66-71). SF_6 is known to capture thermal electrons readily in the gas phase to form a negative ion. However, SF_6 has shown an energy barrier to electron transfer reactions (66) and no observed PD for SF_6 has been reported in the literature. These behaviors are attributed to poor Franck-Condon factors for the neutral and the anion (72, 73).

PD of SF_6

SF_6 responds strongly in the ECD, and attempts were made to measure the PD spectrum of SF_6^- in the PDM-ECD. The resulting δI_M responses observed were very small at λ = 362.5 nm and shorter wavelengths, while no PD was observed at longer wavelengths. The spectrum is shown in Figure 27. The very small size of the δI_M responses produced a high level of uncertainty in the measured cross-section, probably on the order of ± 50%. Due to this great uncertainty, the data has been plotted as a relative cross-section. The absolute cross-section is extremely small, never exceeding 0.03 A^2. In a previous report by Drzaic and Brauman (72), no PD was observed in the ICR with wavelengths down to about 300 nm. However, in an unpublished study by Freiser and Beauchamp (74), a monotonically increasing PD cross-section was observed at shorter wavelengths (350-220 nm). This is not unlike the results obtained with the PDM-ECD.

From the PD data, an E_{th} = 78.9 kcal/mol can be obtained from the λ_{th} = 362.5 nm value. This is in sharp contrast to a reported value of EA = 24.2 kcal/mol obtained from electron transfer equilibria studies (65). However, this very high determination for E_{th} by the PDM-ECD method is consistent with the observed unusual PD behavior of SF_6.

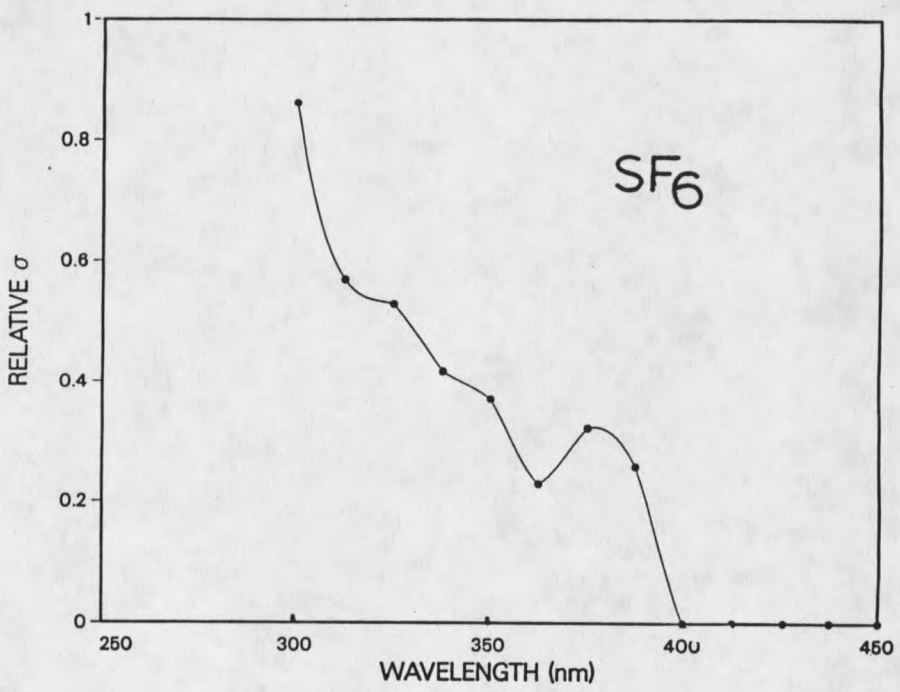

Figure 28. PD spectrum of SF_6 obtained with the PDM-ECD. A relative cross-section scale has been used since the δI_M responses were very small, creating a large uncertainty in the determinations of the σ values, which never exceed 0.03 $Å^2$.

The unexpected PD behavior of SF_6 can be explained by the model discussed previously and represented in Figure 18. The very small PD cross-sections and very high λ_{th} value would indicate large geometry differences between SF_6 and SF_6^-. Hay (73) has recently reported SCF calculations based on an octahedral structure for neutral SF_6 and an assumed octahedral structure for SF_6^- where the bonds are weakened and lengthened; R_e (SF_6) = 1.567 A vs $R_e(SF_6^-)$ = 1.710 A. These results predict an adiabatic EA = 20.8 kcal/mol. However, the vertical PD transition requires much higher energy. A representation based on Hay's (73) work is shown in Figure 29. The

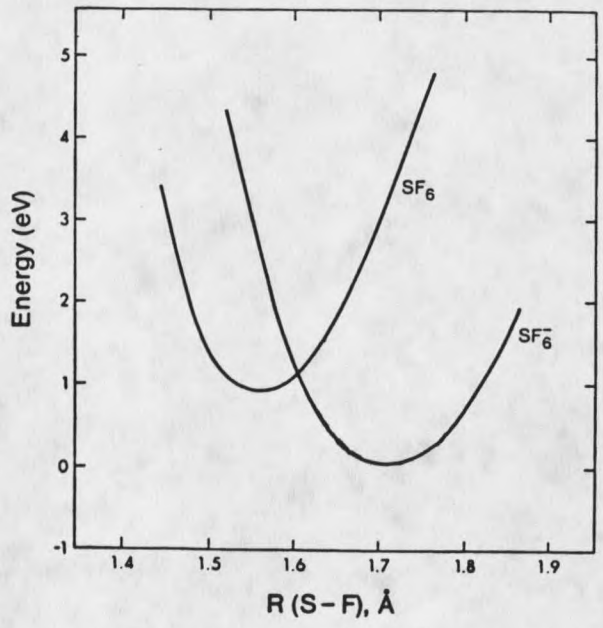

Figure 29. Calculated potential energy curves of SF_6 and SF_6^- as a function of symmetric stretch coordinate from SCF calculations by P.J. Hay (Ref. 73).

potential energy curves shown are in qualitative agreement with the results of Freiser and Beauchamp (74) and the PDM-ECD results. Electron transfer reactions reported by Grimsrud, Chowdhury, and Kebarle (66) indicate a ΔS° = 11 eu for the SF_6^- to SF_6 process, which clearly indicates a large geometry change upon negative ionization. It should also be noted that calculations by Drzaic and Brauman (72) more strongly support a structure for SF_6^- most closely resembling an ion-molecule association complex $(SF_5 \cdot F)^-$, which would also possess poor Franck-Condon overlap for adiabatic photodetachment. This model, however, was based on an EA = 12.5 kcal/mol (75) which is quite low compared to results obtained experimentally by Kebarle and coworkers (66) and calculated by Hay (73).

PD Spectra of Several Perfluoro-cycloalkanes

To date, no known reports have been made on PD from the negative ions of perfluorocycloalkanes. The compounds studied were: C_6F_{12} (perfluorocyclohexane), C_7F_{14} (perfluoromethylcyclohexane), and $C_{10}F_{18}$ (perfluorodecalin). APIMS experiments performed in this lab indicate that the only significant ions formed under ECD conditions are the molecular anions. Two peaks were observed in the chromatogram of $C_{10}F_{18}$, and they were assigned to the cis and trans isomers. The PD spectra of

these compounds are shown in Figure 30. As with SF_6, the PD cross-sections measured by the PDM-ECD for these compounds are quite small, very near the detection limit of the technique. The uncertainty of the cross-sections is so great that the peaks or resonances observed in the spectra may not be real. For C_7F_{14}, a λ_{th} = 387.5 nm leads to E_{th} = 73.8 kcal/mol, much higher than EA = 24.4 kcal/mol determined by Kebarle and coworkers (86) by electron transfer equilibria in the PHPMS experiment. Although the EA values for C_6F_{12} and $C_{10}F_{18}$ are not known, it seems reasonable to speculate that they are similar to that of C_7F_{14}. The large differences between λ_{th} determined by the PDM-ECD experiment and EA determined by electron transfer experiments (66) can be attributed again to poor Franck-Condon factors. Although there are no known reports of calculations for the perfluorocycloalkanes similar to those reported for SF_6 (72, 73), both $C_7F_{14}^-$ and $C_6F_{12}^-$ were found to be extremely unreactive to electron transfer (66, 76).

PD of Perfluorobenzene and Perfluorotoluene

Both C_6F_6 (perfluorobenzene) and C_7F_8 (perfluorotoluene) capture electrons rapidly in the ECD to form negative ions. Sowada and Holroyd (77) have previously reported a PD spectrum for $C_6F_6^-$ in nonpolar solvents. This report showed relatively large cross-